HHS Public Access

Author manuscript

Cell. Author manuscript; available in PMC 2023 January 20.

Published in final edited form as:

Cell. 2022 January 20; 185(2): 283–298.e17. doi:10.1016/j.cell.2021.12.024.

GSDMB is increased in IBD and regulates epithelial restitution/repair independent of pyroptosis

Nitish Rana[1,2], **Giuseppe Privitera**[1], **Hannah C. Kondolf**[1], **Katarzyna Bulek**[3], **Susana Lechuga**[3], **Carlo De Salvo**[1], **Daniele Corridoni**[4], **Agne Antanaviciute**[4], **Rebecca L. Maywald**[5], **Alexander M. Hurtado**[1], **Junjie Zhao**[3], **Emina H. Huang**[6,†], **Xiaoxia Li**[3], **E. Ricky Chan**[7], **Alison Simmons**[4], **Giorgos Bamias**[8], **Derek W. Abbott**[1], **Jason D. Heaney**[5], **Andrei I. Ivanov**[3], **Theresa T. Pizarro**[1,9,*]

[1]Department of Pathology, Case Western Reserve University School of Medicine, Cleveland, OH 44106, USA

[2]Department of Physiology & Biophysics, Case Western Reserve University School of Medicine, Cleveland, OH 44106, USA

[3]Department of Inflammation & Immunity, Learner Research Institute, Cleveland, OH 44195, USA

[4]MRC Human Immunology Unit, MRC Weatherall Institute of Molecular Medicine, John Radcliffe Hospital, University of Oxford, Oxford, United Kingdom

[5]Department of Molecular and Human Genetics, Baylor College of Medicine, Houston, TX 77030, USA

[6]Department of Cancer Biology and Colon & Rectal Surgery Cleveland Clinic Foundation, Learner Research Institute, Cleveland, OH 44195, USA

[7]Institute for Computational Biology, Case Western Reserve University School of Medicine, Cleveland, OH 44106, USA

[8]Academic Department of Gastroenterology, Ethnikon & Kapodistriakon University of Athens, Laikon Hospital, Athens, Greece

[9]Lead Contact

SUMMARY

[*]Correspondence: Theresa Pizarro, Ph.D., Case Western Reserve University School of Medicine, 2103 Cornell Road, WRB 5534, Cleveland, OH 44106, (216) 368-3306, theresa.pizarro@case.edu.

[†]New address: Department of Surgery, University of Texas Southwestern Medical Center, Dallas, TX 75390, USA

AUTHOR CONTRIBUTIONS

NR conceptualized the study, designed/performed experiments, analyzed/interpreted results, wrote and edited manuscript. GP/HCK/KB/JZ/RLM/DC/SL performed experiments, analyzed/interpreted results. AA/ERC were responsible for computational analyses. CDS/AMH performed experiments. EHH/AS/GB/XL/DWA/JDH analyzed/interpreted results, provided reagents. AII designed experiments, analyzed/interpreted results, provided reagents and edited manuscript. TTP conceptualized the study, designed experiments, analyzed/interpreted results, provided reagents, wrote and edited manuscript.

DECLARATION OF INTERESTS

The authors declare no competing interests.

Gasdermins are a family of structurally-related proteins originally described for their role in pyroptosis. Gasdermin B (GSDMB) is currently the least studied, and while its association with genetic susceptibility to chronic, mucosal inflammatory disorders is well-established, little is known of its functional relevance during active disease states. Herein, we report increased GSDMB in inflammatory bowel disease, with single-cell analysis identifying epithelial specificity to inflamed colonocytes/crypt top colonocytes. Surprisingly, mechanistic experiments and transcriptome profiling reveal lack of inherent GSDMB-dependent pyroptosis in activated epithelial cells and organoids, but instead, point to increased proliferation and migration during *in vitro* wound closure, which arrests in GSDMB-deficient cells that display hyper-adhesiveness and enhanced formation of vinculin-based actomyosin stress fibers dependent on PDGF-A-mediated FAK phosphorylation. Importantly, carriage of disease-associated *GSDMB* SNPs confers functional defects disrupting epithelial restitution/repair, which altogether, establishes GSDMB as a critical factor for restoration of epithelial barrier function and the resolution of inflammation.

In Brief

Independently from its established role in pyroptotic cell death, gasdermin B regulates focal adhesion kinase phosphorylation to promote epithelial maintenance and repair. Naturally occurring mutations associated with inflammatory bowel disease disrupt this role.

Keywords

gasdermins; gasdermin B (GSDMB); inflammatory bowel disease; intestinal epithelial cells; epithelial organoids; single cell profiling; RNA-Seq; *GSDMB* genetic polymorphisms; methotrexate (Mtx); platelet-derived growth factor A (PDGFA); focal adhesion kinase (FAK); epithelial restitution and repair; resolution of inflammation

INTRODUCTION

Gasdermins (GSDMs) are comprised of six members (GSDM A-E and DFNB59) that, aside from DFNB59, share sequence homology and are primarily known for their role in pyroptosis(Broz et al., 2020). At present, gasdermin D (GSDMD) is the best characterized of the GSDMs and notably, discovery of its pore-forming capabilities upon cleavage, oligomerization and translocation of the N-terminal effector domain to the plasma membrane has revolutionized fundamental concepts regarding mechanisms of programmed cell death(Shi et al., 2015) and IL-1β secretion(Evavold et al., 2018). Conversely, the precise function and mechanism(s) of action of gasdermin B (GSDMB) remain somewhat elusive, mainly due to limited *in vivo* experimentation attributed to lack of a mouse ortholog, which is unique among other GSDM family members(Broz et al., 2020). Unlike GSDMD, evidence supporting an essential role for GSDMB during pyroptosis is controversial(L. Li et al., 2020), with recent studies indicating requirement of either secondary effector cells (*i.e.*, cytotoxic lymphocytes)(Zhou et al., 2020) or caspase-4(Chen et al., 2019) for cleavage of full-length protein and subsequent activation of pyroptosis in GSDMB-expressing target cells. In fact, much of what has been speculated regarding GSDMB function is based on studies of other family members; however, GSDMB's structure and domain architecture are

reported as one of the most distinct compared to other GSDMs(L. Li et al., 2020), giving rise to the speculation of alternative functions.

Clues uncovering the potential role(s) of GSDMB during health and disease mainly come from GWAS describing SNPs within the protein coding and transcriptional regulatory regions of *GSDMB* that are associated with increased susceptibility of acquiring immune-mediated disorders, including asthma(Moffatt et al., 2007) and inflammatory bowel disease(The International IBD Genetics Consortium (IIBDGC) et al., 2012). Indeed, survey of 27 different healthy tissues shows greatest *GSDMB* abundance in GI-associated organs (*i.e.*, stomach, small intestine, colon)(Fagerberg et al., 2014) and predominant expression in epithelial cells(Saeki et al., 2009). Nonetheless, while more recent reports confirm GSDMB's role in asthma, particularly those describing the influence of, and linkage to, gene polymorphisms on 17q21(Stein, 2018)(X. Li et al., 2020), mechanistic studies regarding disease pathogenesis are severely lacking, with none to date evaluating GSDMB's function in healthy intestinal mucosa and/or during IBD.

IBD, which encompasses Crohn's disease (CD) and ulcerative colitis (UC), is characterized by chronic, relapsing inflammation of the gastrointestinal tract, resulting in immune-mediated tissue destruction and compromise of intestinal barrier function. CD can occur anywhere along the GI tract and can penetrate transmurally, while UC is limited to the colonic mucosa. Although the precise etiology is currently unknown, it is well accepted that IBD develops from dysregulated mucosal immune responses to environmental factors in genetically-susceptible individuals. To date, there is no known cure for IBD; rather, current treatment modalities are aimed at controlling symptoms and achieving long-term remission(Pouillon et al., 2020). A key physiological process that promotes restoration of normal organ function and maintenance of intestinal homeostasis is the resolution of inflammation, of which intestinal epithelial cells (IECs) are central players due to their anatomical location and complex interaction(s) with both the underlying mucosal immune system, as well as the local gut microenvironment. In fact, dysfunction and/or delay in mucosal healing has been implicated in the development of IBD, as well as other chronic inflammatory disorders(Leoni et al., 2015), wherein IECs fail to undergo appropriate repair and restitution, ultimately resulting in compromised barrier integrity. Currently, no treatment modalities exist that specifically enhance and/or improve gut barrier function; however, the intestinal epithelium represents a promising therapeutic target for IBD that remains a very active area of research and development(Odenwald and Turner, 2017).

Herein, we provide a comprehensive report characterizing the expression and potential function of GSDMB in IBD. GSDMB is upregulated and most prevalently expressed in IECs, specifically colonocytes/crypt top colonocytes, from both CD and UC patients with active disease compared to healthy controls. Importantly, our data show a lack of direct GSDMB-dependent programmed cell death (*i.e.*, pyroptosis) in IECs and epithelial organoids, but instead, point to its functional importance in promoting epithelial migration and regulating cell adhesion, adding depth to the literature regarding its role during epithelial proliferation. We also mechanistically address the translational relevance of *GSDMB*'s disease-associated SNPs(Chao et al., 2017) and demonstrate key functional differences from wild-type *GSDMB*. Specifically, introduction of changes from glycine to arginine at

position 299 and from proline to serine at position 306 in *GSDMB* markedly dampens IEC proliferation and migration, but profoundly enhances epithelial adhesion by impeding phosphorylation of the key focal adhesion protein, FAK (focal adhesion kinase), through a mechanism that involves PDGF-A that together, promotes impaired wound healing. These effects can be partially overridden by pharmacologically-targeting phosphorylation of FAK. In summary, our results show IBD-specific upregulation of epithelial-derived GSDMB, a function that is overall protective in nature, yet introduction of disease-associated *GSDMB* SNPs confers functional alterations that mechanistically affect IEC processes critical for restoration of barrier integrity and the resolution of inflammation.

RESULTS

GSDMB is increased during IBD, specifically in IECs that show enriched gene pathways associated with cell proliferation, migration and adhesion, but not pyroptosis

To initially screen for GSDMB in IBD, the GSE database was mined using two separate datasets of endoscopically-procured gut mucosal biopsies from both CD and UC patients (Table S1). Overall, *GSDMB* is increased in inflamed mucosa from different anatomical locations (*i.e.*, terminal ileum, as well as ascending, descending and sigmoid colon) in CD, with more striking differences observed at the same site of consecutive active and remission stages of disease during UC, compared to non-inflamed, location-matched healthy controls (Figure 1A). To expand these studies, macroscopically-involved and non-involved biopsies from individual CD and UC patients (Table S2) were assayed, with results confirming substantial increases in *GSDMB* compared to non-inflamed, healthy controls, and a consistent trend of elevated *GSDMB* in involved vs. non-involved patient-matched samples (Figure 1B, *left*). At the protein level, robust expression of full-length (FL), and to a lesser extent, cleaved, GSDMB is present in gut mucosal biopsies from both CD and UC compared to non-inflamed, healthy controls (Figure 1B, *right*) indicating abundant pooled sources of GSDMB-FL, of which partial cleavage occurs during IBD in both involved and non-involved areas (Figure S1A).

Immunolocalization experiments were performed on surgically-resected full-thickness intestinal tissues from IBD patients compared to non-inflamed, healthy margins of patients undergoing therapeutic bowel resection for malignant and other non-malignant, non-inflammatory conditions, to determine the precise cellular source of increased GSDMB in IBD. The results show intense staining in ileal and colonic specimens from CD and UC patients, respectively, that mainly localizes to IECs, with little to any expression in controls (Figure 1C, *left*). Interestingly, presence of GSDMB in restituting epithelium, characterized by undifferentiated, single-layer IECs overlying areas of active inflammation and granulation tissue, commonly found in IBD (Figure 1C, *arrows*), suggests its role in mucosal healing. Co-localization of GSDMB (*red*) with the epithelial-specific cell surface marker, EpCAM (*green*) (Figure 1C, *right*), confirms expression to the epithelium, specifically along the plasma membrane in inflamed IBD tissues (Figure 1C, *arrowheads*). In further support of these findings, freshly isolated IECs from non-resolving CD and UC patients (Table S2) show dramatic increases (5.09-fold and 5.83-fold, respectively) in *GSDMB* compared to non-inflamed healthy controls (Figure 2A, *left*). Corresponding

protein levels are also consistent with that observed in unfractionated gut mucosal tissues, with robust expression of IEC-derived GSDMB-FL in CD and UC compared to controls, but notably, in the absence of cleaved forms (Figure 2A, *right*, Figure S1B).

Next, to further identify *GSDMB*-expressing IEC subpopulations, a supervised analysis was performed on a previously published large-scale scRNA-Seq dataset compiled from profiled IECs, isolated from inflamed and non-inflamed areas of active, immunomodulatory-naïve UC patients and from normal, non-inflamed healthy controls, in which IEC subpopulations unique to IBD were reported (Figure S1D)(Parikh et al., 2019). Results reveal differential distribution and distinct differences in relative *GSDMB* among IEC subtypes (Figures 2B–C), predominantly in colonocytes, crypt top colonocytes, and to a lesser extent, goblet cells, with a general increase in inflamed vs. non-inflamed and healthy controls (Figure 2C). Upregulated Gene Ontology (GO) biological processes were evaluated in *GSDMB*-expressing colonocyte and crypt top colonocyte subpopulations, showing prevalence of gene enrichment pathways associated with, proliferation, migration and adhesion (Figure 2D), but surprisingly, lacking those related to pyroptosis or cell-lysis. Together, our results represent a comprehensive characterization of GSDMB in IBD, showing increased GSDMB, primarily localized to IECs and indicate potential, functional importance in non-pyroptotic roles.

Methotrexate (Mtx) induces upregulation of IEC-derived GSDMB-FL and translocation to the plasma membrane, but not lytic cell death

The unexpected lack of enriched gene pathways identified with pyroptosis in our scRNA-Seq analysis prompted further investigate of GSDMB-dependent functions, importantly dissecting its role in the absence of confounding inflammation. A fundamental issue pervading the field of gasdermin biology has been to identify the mechanism(s) by which GSDMB can be increased *in vitro*(Broz et al., 2020)(L. Li et al., 2020). To this end, evaluation of several IEC lines was performed, selecting undifferentiated HT-29 cells, a human adenocarcinoma colorectal cell line, for its ability to endogenously express GSDMB (Figure S2A) and to serve as a suitable transfection host. Moreover, after testing a wide array of inflammatory mediators known to be involved in the development of IBD (Figure S2B), and using a public repository of high-throughput functional genomic data analyzing potential molecules regulating GSDMB (*i.e.*, GEO, NIH), methotrexate (Mtx) was identified as an inducer of GSDMB-FL, but of note, did not execute its cleavage, similar to IFNγ(Zhou et al., 2020) (Figures S2C–D). Mtx is a multi-function drug, best known to inhibit purine and pyrimidine synthesis and target proliferation of T lymphocytes(Cronstein and Aune, 2020), whereas little is known regarding its effect(s) on IECs(Jeffes et al., 1995). Immunolabelling of GSDMB in HT-29s demonstrates upregulation of its expression, and importantly, translocation to the lateral plasma membrane, where it is adjacent to, and/or co-localizes with, the basolateral plasma membrane marker, E-cadherin, in a punctate pattern upon stimulation with Mtx (Figure 3A, *middle*, *arrowheads*), but not with IFNγ (Figure 3A, *lower*). Subcellular fractionation displays consistent results with this finding, showing increased GSDMB-FL in IEC membrane and organelle fractions upon exposure to Mtx vs. IFNγ or untreated controls (Figure 3B). These results are confirmed in colonic epithelial organoids (Table S2), in which GSDMB increases after exposure to Mtx and IFNγ, but co-localizes (*arrowheads*) with EpCAM only after Mtx stimulation (Figure 3C).

Remarkably, Mtx- and IFNγ-induced GSDMB expression does not induce IEC cytotoxicity, measured by lack of LDH (lactate dehydrogenase) release, in either WT HT-29 or GSDMB knockout (*GSDMB*$^{-/-}$) cells (Figure S3A–E), compared to untreated controls (Figure 3D). These results are confirmed in epithelial organoids upon Mtx stimulation, in contrast to GSDMD-dependent activation of NLRP3 inflammasomes by LPS plus nigericin that predictably triggers significant cell death(Mehto et al., 2019), indicated by uptake of SYTOX™ deep red stain (Figure 3E, *arrowheads*). Association between cell death and GSDMB expression was examined via processing and cleavage of pyroptotic caspase 1 (Figure S2E and F), in addition to cleavage of initiator caspase 8, and executioner caspases 3 and 7, all of which yielded negative results in WT and *GSDMB*$^{-/-}$ cells, with or without GSDMB upregulation (Figures S2G–I). Together, these data indicate that, despite its ability to upregulate and translocate GSDMB-FL to the cell membrane and cell membrane-associated organelles, Mtx does not appear to induce GSDMB-dependent cell death by pore formation, which may be attributed to its failure to cleave GSDMB-FL.

To further address this issue, either GSDMB-NT or GSDMB-FL was overexpressed in HEK293T cells, which lack endogenous expression of any gasdermins(Zhou et al., 2020), and compared to cells overexpressing GSDMD-NT (Figure S4A–C) that effectively induces cell death by autolytic pore formation(Shi et al., 2015). Unlike GSDMD-NT, neither GSDMB-NT nor GSDMB-FL has the ability to induce cell cytotoxicity (Figure 3F), and neither shows evidence of pore formation, measured by propidium iodide (PI) uptake (Figures 3G,S4D), a hallmark feature of pyroptosis leading to eventual cell lysis(Ding et al., 2016). These results suggest that other GSDMB-dependent, non-pyroptotic function(s) may be important, and likely occur, in IECs.

GSDMB regulates IEC proliferation and migration

In line with our scRNA-Seq results (Figure 2D) and following an unsupervised cluster analysis of RNA-Seq expression data comparing *GSDMB*$^{-/-}$ vs. WT HT-29s, we found significant enrichment of GO pathways associated with proliferation, migration and adhesion (Figures S5A–B). These are key IEC functions that are essential for maintenance of the normal gut barrier under homeostatic conditions and barrier restitution during mucosal inflammation. Heatmaps demonstrate global, yet distinct, differences in expression of genes related to proliferation and migration comparing *GSDMB*$^{-/-}$ vs. WT HT-29s (Figures S5C–D). Applying more strict statistical criteria (log2FC≥2) (Figure 4A), differential gene expression of molecules related to decreased epithelial proliferation is observed in *GSDMB*$^{-/-}$ compared to WT HT-29s, including *CDX2*, *CDKN1A, HOXD13, MTSS1, PHLDA2, and HLA-DMB* (Figure 4B) which represent the greatest, differentially expressed genes (Table S3). Functionally, cells lacking GSDMB demonstrate a marked reduction in baseline proliferative activity compared to controls (by approximately 45%) and while stimulation with Mtx, but not IFNγ, causes a modest, yet significant, increase, these responses are generally dampened in *GSDMB*$^{-/-}$ cells (Figure 4C).

Because wound repair requires sequential phases of proliferation and migration(Gurtner et al., 2008), we next evaluated GSDMB's potential role in contributing to *in vitro* wound healing, and found that lack of GSDMB substantially impedes IEC wound closure in

WT HT-29s (by 57%), as well as after Mtx or IFNγ treatment (by 68 and 48%), and is accelerated in WT cells upon stimulation with Mtx (by 24%), but not with IFNγ (Figure 4D). In fact, heatmap clustering of genes associated with epithelial migration, such as *CX3CL1*, *AGT*, *CSPG4*, *ROBO1*, and *TGFB1*, reveal significant differences comparing *GSDMB*$^{-/-}$ IECs and WT HT-29 cells, and point to decreased migration in the absence of GSDMB (Figures 4E–F, Table S3). Boyden Chamber migration assays functionally show that lack of GSDMB potently decreases the ability of IECs to effectively migrate compared to WT HT-29s, even in the absence or presence of either Mtx or IFNγ (by 57%, 54%, and 55%, respectively; Figure 4G). Overall, these data further support GSDMB's role in IEC proliferation, while highlighting its contribution to GSDMB-dependent epithelial cell migration.

Lack of GSDMB results in hyper-adhesiveness of IECs

Extracellular matrix adhesion represents an important mechanism impacting cell migration and overall cell motility(Ridley, 2003). In line with the previous observations, heatmap gene clustering of adhesion-related molecules are significantly altered in *GSDMB*$^{-/-}$ compared to WT HT-29 IECs (Figure S5E), and include *CDH17, CD99, GAS6, KIF26B, GPC4 and CAV1* (Figures 5A–B, Table S3). Network analysis generated with central nodes of proliferation, migration and adhesion, showcase differentially expressed genes with log2FC>2 and highlight their interconnections (Figure 5C). Functionally, adhesion is markedly enhanced in *GSDMB*$^{-/-}$ cells vs. WT controls (by 20%) and further increases with Mtx (by 37%) (Figure 5D). To gain better insight into the molecular mechanisms underlying this GSDMB-dependent phenotype, immunofluorescent labeling of wound-activated HT-29 cells was performed for vinculin, a molecule associated with cell-matrix adhesion(Bays and DeMali, 2017), and non-muscle myosin IIA (NM IIA), providing contextual structural morphology for the leading edge of the inflicted wound. Our results reveal the emergence of vinculin-based focal adhesions in *GSDMB*$^{-/-}$ cells when stimulated with Mtx, which are increased compared to WT (Figure 5E, *arrows*). Together, we show that lack of GSDMB results in a hyper-adhesive IEC phenotype that impairs the overarching process of epithelial wound closure.

Rescue of *GSDMB*$^{-/-}$ IECs with IBD-associated mutant vs. WT GSDMB dampens *in vitro* IEC wounding healing-type functions

To date, the most compelling data linking GSDMB to IBD comes from GWAS, revealing strong genetic association in regions of chromosome 17q21, corresponding to *GSDMB*, with increased susceptibility to IBD(The International IBD Genetics Consortium (IIBDGC) et al., 2012). Two candidate SNPs (rs2305479 and rs2305480) include a change from glycine to arginine at position 299 and from proline to serine at position 306, respectively, (*GSDMB*$^{\Delta R299:S306}$), which together, is speculated to confer decreased conformational flexibility and a greater positive surface charge compared to WT GSDMB (*GSDMB*$^{G299:P306}$), based on differences in their crystal structure(Chao et al., 2017). Interestingly, preliminary findings indicate that carriage of mutant *GSDMB*$^{\Delta R299:S306}$ confers increased *GSDMB* in gut mucosal biopsies derived from IBD patients as well as healthy controls, compared to WT *GSDMB*$^{G299:P306}$ (Figure S1C).

To assess the functional relevance of these SNPs, specifically in IECs, we utilized *GSDMB*$^{-/-}$ (KO) cells and developed rescued cell lines that stably express GSDMB encoded by either mutant or canonical WT *GSDMB*, with GSDMB KO cells transfected with empty vector serving as control (Cont.) (Figure S3F–H). RNA-Seq comparing IECs rescued with WT vs. mutant *GSDMB* once again show significant enrichment of differentially expressed genes related to proliferation, migration and adhesion (Figure 6A). Functionally, both GSDMB-overexpressing IEC lines demonstrate markedly increased proliferation compared to control. However, mutant *GSDMB*$^{\Delta R299:S306}$ IECs show a slight, although significant, decrease in proliferative activity compared to *GSDMB* WT (Figure 6B). In line with these results, carriage of mutant *GSMDB* in colonic epithelial organoids derived from UC patients show less proliferation compared to WT, measured by DNA synthesis staining with EdU, which further decreases in WT *GSDMB* KD (knockdown) organoids (Figure S6A–B). Measurement of *in vitro* wound healing reveals more striking results, in which *GSDMB*$^{-/-}$ cells rescued with *GSDMB* WT exhibit accelerated wound closure vs. mutant *GSDMB*$^{\Delta R299:S306}$ and Cont. (by 32% and 75%, respectively), even after Mtx (Figure 6C), which was recapitulated in WT vs. mutant and in WT *GSDMB* KD organoids (Figure S6C). Moreover, migration of mutant *GSDMB*$^{\Delta R299:S306}$ IECs is dampened (by 47%) (Figure 6D), while adhesion is significantly increased (Figure 6E) compared to *GSDMB* WT, similar to what is observed in organoids carrying the mutant *GSDMB* variants vs. WT *GSDMB*, which is further enhanced when *GSDMB* is knocked down (Figure S6D). Expectedly, co-localization of NM IIA and vinculin in control IEC lacking GSDMB highlight the presence of vinculin-based focal adhesion stress fibers (Figure 6F, *upper*), which are virtually absent in rescued *GSDMB* WT IECs (Figure 6F, *middle*). However, robust formation of these vinculin-based adhesion stress fibers is evident in mutant, IBD-associated *GSDMB*$^{\Delta R299:S306}$ IECs (Figure 6F, *lower*). These results are consistent with observations of UC organoids carrying either WT or mutant *GSDMB*, which show enhanced stress fibers (*arrows*) after stimulation with Mtx (Figure S6E). Together, these results indicate that carriage of *GSDMB*-associated IBD SNPs confers functional IEC alterations associated with decreased proliferation and migration, and enhanced adhesion, which together, hamper epithelial restitution/repair processes important during mucosal wound healing.

GSDMB-mediated regulation of FAK phosphorylation promotes IEC restitution and repair

To better understand potential mechanism(s) involved in GSDMB-mediated regulation of efficient IEC restitution, we interrogated a battery of adhesion-related molecules (Figure S7A), which are important, and known, regulators of focal adhesion dynamics (Figure S7B). Our results show a specific decrease of FAK phosphorylation in *GSDMB*$^{-/-}$ vs. control WT cells, which has been reported to considerably enhance cell adhesion(McLean et al., 2005), with no change in baseline, unphosphorylated FAK (Figures 7A, S7C). Phosphorylated FAK is decreased in IECs rescued with mutant *GSDMB*$^{\Delta R299:S306}$, similar to control IECs lacking *GSDMB*, compared to *GSDMB* WT (Figures 7B, S7D), Using a small molecule drug, ZINC40099027, that serves as an allosteric activator of FAK phosphorylation (Rashmi et al., 2021) (Figure S7E), *in vitro* epithelial wound closure of treated WT, but not *GSDMB*$^{-/-}$, IECs is dramatically increased, whereas wound closure is accelerated in rescued *GSDMB* WT, and to a lesser extent in mutant *GSDMB*$^{\Delta R299:S306}$

(Figure 7C). Heatmap of differentially expressed genes from RNA-Seq of *GSDMB*$^{-/-}$ vs. WT HT-29s, in fact, show clustering of molecules related to regulation and/or function of FAK (Figure 7D), including *PDGFA,* a polypeptide growth factor demonstrated to phosphorylate FAK(Singh et al., 2019)(Hunger-Glaser et al., 2004), which was analyzed to be of greatest statistical significance compared to all modulated genes (Figure 7E). PDGF-AA protein expression (one of two ligands encoded by the *PDGFA* gene) was confirmed to be dependent upon GSDMB expression, rescued by WT *GSDMB,* and to a lesser extent by *GSDMB*$^{\Delta R299:S306}$ (Figure 7F), whereas PDGF-AB did not display significant trends dependent upon *GSDMB* (Figure S7F). Upon stimulation with recombinant PDGF-AA, FAK phosphorylation was observed to increase in WT HT-29s, but more significantly in *GSDMB*$^{-/-}$ cells(Figure 7G), prompting rescue of the deficiency in epithelial *in vitro* wound closure (Figure 7H). Overall, these data further support GSDMB's role in proliferation, while highlighting GSDMB-dependent functions of cell migration and adhesion, with changes in FAK phosphorylation modulated by PDGF-A, that globally affects cell motility, and the overall process of epithelial restitution and repair (Figure 7I).

DISCUSSION

Although the current literature indicates an undeniable link between GSDMB and genetic susceptibility to asthma and IBD, functional studies are limited due to the lack of *in vivo* models. An exception is the study by Das *et al.*, in which bronchoprovocation of mice genetically-engineered to overexpress the human GSDMB-FL transgene (*i.e.*, h*GSDMB*$^{Zp3\text{-}Cre}$ strain) showed airway hyperresponsiveness and remodeling after methacholine exposure (in the absence of inflammation), which could be exacerbated upon challenge with house dust mite allergens that also induced potent Th2 immune responses and asthma-like symptoms(Das et al., 2016). Pyroptosis was not investigated in this study, and since these mice were contrived to globally-produce GSMDB, it is unclear whether the aforementioned effects are specifically due to overexpression of IEC-derived GSDMB or an orchestration of several different cell types that may, or may not, normally produce GSDMB. It should be noted, however, that h*GSDMB*$^{Zp3\text{-}Cre}$ mice appear to develop normally, and under homeostatic conditions, no phenotypic pathologies were reported when compared to WT controls(Das et al., 2016), although the GI tract was not specifically examined for baseline inflammation and/or other gut-related abnormalities.

While GSDMB-related research has been more active in asthma, the present study fully characterizes GSDMB in patients with both CD and UC, the two idiopathic forms of IBD. In line with other disease states, we show that in IBD, the major source of GSDMB is IECs, particularly from inflamed lesions, with single-cell profiling determining specificity to colonocytes and crypt top colonocytes, known to be functionally essential for absorption, and more recently described to express upregulated inflammatory pathways across these cell clusters(Parikh et al., 2019). Upon further analysis of *GSDMB*$^{+}$ colonocytes/crypt top colonocytes, we found enriched gene pathways associated with proliferation, migration and adhesion, but surprisingly, not programmed cell death/pyroptosis, which led us to pursue potential GSDMB-dependent mechanism(s) focused on epithelial restitution and mucosal wound healing. Interestingly, across all IEC subtypes, we recently showed increased *GSDMD* also in colonocytes and crypt top colonocytes from inflamed IBD lesions(Bulek

et al., 2020), suggesting probable interaction(s) and cooperativity of these two gasdermin family members, at least in particular subpopulation of IECs, that may contribute to IBD pathogenesis. Further investigation is warranted to probe this potential relationship.

Of note, while it is well-accepted that GSDMD is required, the contribution of GSDMB during pyroptosis and subsequent cell lysis remains a contested issue(L. Li et al., 2020). Earlier studies suggest alternative, non-pyroptotic (mainly proliferative) functions, whereas more recent studies point to pyroptosis, but by non-conventional mechanisms that are dependent upon either caspase-4(Chen et al., 2019), or a two-step process relying on the interaction with cytotoxic lymphocytes(Zhou et al., 2020). In the latter, electroporation or release of pore-forming perforin after co-culture with either cytotoxic T lymphocytes or NK cells allows access of granzyme A into GSDMB-expressing target cells, which cleaves and activates GSDMB-FL, resulting in pyroptosis(Zhou et al., 2020). Although our data points to inherent, *non*-pyroptotic function(s), GSDMB-dependent IEC pyroptosis cannot be ruled out as a potential pathogenic mechanism during IBD. Indeed, while GSDMB-FL remains the major isoform, cleaved fragments are also clearly present in IBD intestinal biopsies (comprised of several mucosal cell types), in involved and non-involved lesions, but are virtually absent in freshly isolated IECs from all patients groups. As such, while inflammation, for example, may provide the trigger for GSDMB-dependent pyroptosis, which may or may not require auxiliary immune cells, other roles for GSDMB, particularly its full-length form, may also have functional importance for the gut epithelium.

In the search for non-inflammatory stimuli that could potentially upregulate GSDMB, we mined publicly accessible high-throughput functional genomics data submitted by the research community and ultimately identified Mtx, a folate antagonist and well-established pharmaceutical used to treat inflammatory disorders, such as rheumatoid arthritis(Cronstein and Aune, 2020) and IBD(Herfarth et al., 2016). Although it has long been accepted to impede proliferation of T-lymphocytes by inhibiting *de novo* purine and pyrimidine biosynthesis, alternative mechanisms of action have been recently attributed to Mtx, including, among others, nuclear translocation of NF-κB, activation of JAK-STAT signaling and transmethylation reactions(Cronstein and Aune, 2020). Herein, we report the induction of epithelial-derived GSDMB via Mtx and importantly, make the observation that Mtx promotes GSDMB translocation to the plasma membrane, interestingly only in its full-length form, which together makes Mtx a useful to regulate GSDMB without the confounding factors associated with inflammation. In regards to inflammatory stimuli, however, IFNγ was also recently described to markedly upregulate GSDMB(Zhou et al., 2020), which we confirm, but unlike Mtx, it does not elicit translocation to membrane-bound organelles or the plasma membrane. We also confirm the ability of IFNγ alone to promote cell cytotoxicity and robustly induce caspase-1(Detjen, 2001); however, these effects are independent of GSDMB.

Importantly, our data highlight a previously unrecognized function of GSDMB in regulating IEC migration, a required process for effective epithelial restitution and repair that is particularly critical for IBD patients to promote healing of mucosal wounds and ulcerations during remission phases of disease. Epithelial wound healing is a collective process orchestrated by a variety of mechanisms, but primarily coordinates proliferation and

migration of cells, and requires critical interactions between cell-cell and cell-matrix adhesions(Leoni et al., 2015). Our reported effects of GSDMB on IEC migration appear to be independent from regulation of cell proliferation and involves control of cell-matrix adhesion; specifically, loss of GSDMB results in cell hyper-adhesiveness, which impedes cell motility. Enhanced GSDMB-dependent matrix adhesion is associated with the increased assembly of vinculin-based focal adhesions. This is likely due to PDGF-A dependent inactivation (de-phosphorylation) of FAK, a key tyrosine kinase that regulates focal adhesion turnover and linkage to the cytoskeleton(Schaller, 2010)(Hu et al., 2015). PDGF-A is one of four growth factors and is a well-established modulator of cellular proliferation(Chen et al., 2013), but importantly, of actin reorganization and phosphorylation of FAK(Singh et al., 2019), specifically at site Tyr-397, the area of our focus (Hunger-Glaser et al., 2004). We found that GSDMB KO IECs rescued with IBD-associated *GSDMB* SNPs decrease phosphorylation of FAK and increase formation of vinculin-based actomyosin stress fibers, together enhancing adhesion and phenotypically resembling IECs lacking GSDMB. Furthermore, using a small drug-like FAK allosteric activator, ZINC40099027, in addition to recombinant PDGF-AA, we confirm the importance of FAK phosphorylation for GSDMB-mediated *in vitro* wound closure, which represents an interesting therapeutic target to enhance epithelial restitution and repair, similar to other effector molecules impacting epithelial barrier integrity and function, including MLCK1, that has shown success in pre-clinical models of IBD(Graham et al., 2019). Our study presents conceptually the functional consequences of carriage of disease-associated *GSMDB* SNPs in that, aside from increased adhesion, decreased migration and to a lesser extent, proliferation, as well as overall hampered *in vitro* wound healing, occurs in IEC. These results complement a recent study reporting conformational changes in the crystal structure of GSDMB-FL that cause an altered charge on protein surface loop, and subsequent structural rigidity, of mutant GSDMB(Chao et al., 2017). In the same study, GSDMB-FL binding to phosphoinositides and sulfatides(Chao et al., 2017), commonly enriched within intracellular plasma/organelle and apical membranes of epithelial cells, respectively, was observed, which, along with our data demonstrating GSDMB-FL translocation to membrane-associated cell structures, suggests that mutant GSDMB may impede the efficiency of epithelial motility during restitution.

In conclusion, we report functions of full-length GSDMB that involves epithelial restitution and repair via cellular proliferation, migration and adhesion, and modulation of FAK phosphorylation that in part is regulated by PDGF-A. Future studies investigating potential downstream targets of GSDMB will be critical to better understand the molecular mechanisms of these processes, especially differences attributed to disease-associated *GSDMB* SNPs. Our findings provide the foundation to develop therapeutic strategies that target GSDMB to potentially improve epithelial restitution/repair and the resolution of inflammation, with the goal of more effectively treating disorders affecting barrier function, such as IBD.

Limitations of the Study

While GSDMB lacks a mouse ortholog, future studies utilizing animal models of IBD that transgenically-express h*GSDMB* may provide more clarity regarding its role in an *in*

vivo setting. Preliminary data regarding IBD biopsy samples expressing mutant *GSDMB* (containing SNPs correlated with increased risk of asthma and IBD) also needs to be further expanded using large patient populations to better define a definitive association between mutant vs. WT *GSDMB* in regards to IBD phenotype and disease progression. Additionally, while the present study has provided a better understanding regarding the mechanism by which GSDMB-dependent function(s) in IECs impact IBD pathogenesis, at the same time, it has also instigated compelling questions to pursue for future investigation. For example, what is GSDMB's precise role in IL-1β processing and secretion, and do GSDMB-FL vs. -NT proteins impart functional differences that impact fundamental epithelial biology? Furthermore, the downstream targets of GSDMB, including FAK and PDGF-A, represent one pathway that promotes epithelial restitution and repair; however, restoration of intestinal barrier function is a multifactorial process and likely encompasses other GSDMB-dependent molecular signaling events that requires further study.

Finally, an important conceptual issue that cannot be ignored is that both IBD and asthma are disorders that affect organs directly interfacing with the external environment and their associated microbiomes(Budden et al., 2017). In fact, the emerging role of gasdermin family members within the context of infection has centered upon host defense(Tang et al., 2020); however, in regards to GSDMB, little is known concerning the impact of infection and/or the microbiome. Earlier work reported increased *GSDMB* after rhinovirus infection(Çalışkan et al., 2013), while a more recent study elegantly showing that after *Shigella* infection, GSDMB can selectively form pores in bacterial-derived membranes and promote microbicidal activity, while protecting host IECs from undergoing pyroptosis(Hansen et al., 2021). Further investigation regarding the potential role(s) of GSDMB during host-microbiome interaction(s) are warranted and will likely uncover important, functional mechanism(s) in mucosal-associated diseases, such as IBD.

STAR METHODS

RESOURCE AVAILABILITY

Lead contact.—Further information and requests for resources should be directed to, and will be fulfilled by, the lead contact, Theresa T. Pizarro (theresa.pizarro@case.edu).

Materials availability.—Plasmids, primers, recombinant protein, genetically-engineered cell lines, and any other research reagents generated by the authors will be distributed upon request to other research investigators under a Material Transfer Agreement.

Data and code availability.—scRNA-Seq: all raw and processed next-generation sequencing data has been deposited with GEO and are publicly available as of the date of publication. Accession numbers are listed in the key resource table.

RNA-Seq: all raw and processed next-generation sequencing data has been deposited with GEO and publicly available upon acceptance of publication. The accession number is listed in the key resource table.

EXPERIMENTAL MODEL AND SUBJECT DETAILS

Human subjects.—Surgically-resected intestinal tissues, gut mucosal biopsies and freshly-isolated IECs were harvested and/or processed as previously described(Pastorelli et al., 2010), and obtained from the Biorepository Core of the NIH-sponsored Cleveland Digestive Diseases Research Center (DDRCC) and the Endoscopy Unit of the first Department of Internal Medicine, Propaedeutic, at Laikon Hospital (Athens, Greece). Samples were taken from areas with evident macroscopic inflammation (involved), and normal-appearing mucosa (non-involved), with confirmed histopathologic diagnoses of either CD or UC. Patients undergoing therapeutic bowel resection for malignant and other non-malignant, non-inflammatory conditions and individuals undergoing screening colonoscopy, who did not display endoscopic and histopathological mucosal abnormalities, served as controls. Age and sex of subjects can be found in Table S2. Tissues were used for: IHC, as described below, cultivation of colonic epithelial organoids, as described below, or maintained at either 4°C for 1–2d in RNA*later*™ solution until further processing or storage at −80°C, and subsequently used for total RNA isolation/qPCR and protein extraction. All studies were approved by the appropriate Ethics Committees of the Cleveland DDRCC, Cleveland Clinic Foundation (CCF), and Laikon Hospital. Informed consent was obtained from all subjects.

Human cell lines.—HT-29 cells (human; sex: female, colonic epithelial) were cultured in McCoy's 5A medium modified with L-glutamine and sodium bicarbonate, supplemented with 10% FBS and 2% penicillin/streptomycin. HEK293T cells (human; sex: female, kidney epithelial) were grown in Dulbecco's Modified Eagle Medium (DMEM) supplemented with 10% SuperCalf serum and 1% antibiotic/antimycotic. Intestinal epithelial organoids were derived from the colon of IBD and control patients as previously described(Sarvestani et al., 2018); age and sex of subjects can be found in Table S2. Organoid cultures were cultivated in Matrigel® using 50% Advanced DMEM and 50% conditioned media, conditioned by Wnt3a, R-spondin 3 and Noggin (L-WRN) L-cells, prepared according to (Miyoshi and Stappenbeck, 2013) Generation and maintenance of 2D monolayers from 3D organoids were followed as previously described(Reed et al., 2019), and used for subsequent functional assays. All cell lines were grown at 37°C under 5% CO_2. Cell lines were authenticated by STR profiling and assayed for mycoplasma contamination using LookOut Mycoplasma PCR Detection Kit.

METHOD DETAILS

in vitro stimulation of intestinal epithelial cells.—HT-29 cells or colonic epithelial organoids were grown to 70% confluency in complete media, with or without either; Mtx (10uM/mL for 24h), human recombinant (hr)IFNγ (10ng/mL for 24h), hrTGFβ, hrTNF (both at 50ng/mL for 12h), hrIL-33 (100ng/mL for 6h), flagellin (500ng/mL for 6h), DSS (2% for 4h), ZINC40099027 (10nM for 24h) or hrPDGF-AA (10ng/mL for 24h). Serum starved cells (2h) were stimulated with LPS (1 μg/mL for 4h), followed by nigericin (10μM for 1.5h) in Hank's Balanced Salt Solution (HBSS) supplemented with 1% FBS and MEM Amino Acid Solution. Supernatants were immediately collected, aliquoted and frozen at −20°C for subsequent assays; cells were harvested for total RNA or protein extraction as described below.

Immunolabeling.—Gut mucosal biopsies (collected as previously described) were rinsed, examined for gross morphological changes, and a representative full-thickness sample was obtained. Tissues were fixed in 10% buffered formalin phosphate for 24h at RT, followed by dehydration in 3 separate 70% ethanol washes, and subsequently stored in 70% ethanol for 2–7d. Samples were then embedded in paraffin and resulting blocks were stored at room temperature for later tissue sectioning. Five-micron-thick serial sections were obtained and mounted on poly-L-lysine coated Superfrost/Plus glass slides. Slides were heated to 60°C for 20 min, followed by two 5-min washes in xylene to deparaffinize and single 5 min washes in 100%, 95%, 70% to dehydrate. Tissue sections were then permeabilized for 30 min with saponin buffer (0.5% saponin in PBS) and blocked for endogenous peroxidase using 1% H_2O_2 in saponin buffer for 30 min. Sections were blocked for 30 min with normal goat serum for 30 min and incubated with primary GSDMB antibody overnight at 4°C. The following day, slides were washed in PBS and incubated with biotinylated anti-rabbit IgG for 30 min, followed by avidin-biotin complex (ABC) for 30 min. Reactive cells were visualized by adding diaminobenzidine (DAB) substrate and counterstained with hematoxylin. Protocol was followed as previously described(Pastorelli et al., 2010). IHC stained slide images were obtained on an Olympus VS120-S6-W Virtual Slide Microscope. Immunofluorescent labeling for confocal imaging of tissue sections, HT-29 cell monolayers (grown to 100% confluency on glass coverslips) or epithelial monolayer derived from 3D colonoids (described above) was completed as described, with the exception of using an appropriate fluorochrome-conjugated secondary antibody; key resource table. Confocal images were acquired on a Leica TCS SP8 confocal microscope and subsequently processed using Adobe Photoshop.

qPCR.—Total RNA was harvested from HT-29 cells and colonoids using High Pure RNA Isolation Kits and from endoscopic biopsies and freshly isolated IECs using the AllPrep® DNA/RNA/Protein Mini Kits both per manufacturers' protocols. Total RNA was stored at −80°C until 1ug was reverse-transcribed using High-Capacity RNA-to-cDNA™ Kits. cDNA was diluted 4-fold in RT-PCR grade water and stored at −20°C until use. Real-time qPCR was performed using Taqman gene-expressing assays and FastStart Universal Probe Master (ROX); key resource table, as previously described(Lopetuso et al., 2018) or as outlined by manufacturer on QuantStudio 3 Real-Time PCR Systems under ΔΔCT run method. Values were calculated as ratio of GSDMB/GAPDH (housekeeping gene) and expressed as fold-differences vs. Cont. for all experiments.

Western blots.—WCLs were prepared and run as previously described(Bulek et al., 2020) using AllPrep® DNA/RNA/Protein Mini Kits and subcellular fractions using Cell Fractionation Kits, both per manufacturer's protocol. Quantification of protein was completed using Pierce™ BCA Protein Assay Kits. WCL protein for Phospho-FAK analysis was extracted and prepped as described above, except using PhosphoSafe™ Extraction Reagent instead of RIPA. Digital blot exposures were analyzed using ImageQuant™ LAS 4000 and densitometry calculated using Image J software.

SNP genotyping.—Total DNA was harvested from endoscopic biopsies using AllPrep® DNA/RNA/Protein Mini Kits 80004. DNA was quantified by NanoDrop™

spectrophotometry and subsequently used for analysis by commercially available TaqMan® SNP Genotyping Assay single-tube assays using TaqMan® Genotyping Master Mix and specific, predesigned SNP primers for position 299 and 306; key resource table, as per manufacturer's protocol. Results were analyzed using TaqMan® Genotyper Software.

Generation of GSDMB$^{-/-}$ HT-29 cells & GSDMB KD colonic epithelial organoids.—Guide RNA plasmids were generated (Figure S3) as previously described*(Ran et al., 2013)*, and synthesized by Millipore Sigma with the following modifications: NEB Buffer 2.0 was supplemented instead of Tango Buffer and px459 (Puro) plasmid was used. Constructs were transformed into DH5-α and sequenced to confirm colonies. Lipofectamine™ 3000 was used per manufacturer's instruction for transfection of HT-29 cells with 6:1 and 3:2 ratios of Lipofectamine to plasmid, respectively. HT-29 cells were selected with G418 for 5d, with surviving cells used in serial dilutions to be screened as individual clones. Clones were TA cloned using pGEM-T and sequenced for deletion confirmation. A second round of transfection from Lipofectamine™ 3000 onward was employed to remove the third allele. *GSDMB* KD of colonoids employed commercially available shRNA knockdown lentiviral vector for h*GSDMB*; key resource table. Puromycin selection was used as previously described (Miyoshi and Stappenbeck, 2013) to select for GSDMB deficient colonoid cultures.

Generation of GSDMB overexpressing cell lines.—GSDMB, pMD2.G #12259 and psPAX #12260 were a gift from Didier Trono. Gibson assembly was used to subclone GSDMD-NT, GSDMB-NT, and GSDMB-FL into transient or lentiviral vectors (Figure S4). Site-directed mutagenesis was used to create R299G and S306P polymorphisms (Figure S3). All constructs were Sanger-sequence verified. HEK293T cells were seeded overnight in 6-well plates and transfected using calcium phosphate with 1, 2 or 4 μg of plasmid DNA. Four hours post transfection, cells were washed with PBS and changed into fresh media. For lentiviral production, lentiviral plasmids, pMD2.G, and PsPax, were transfected in a 4:3:1.2 ratio in HEK293T cells. After 2d of virus production, supernatant was collected, cleared by centrifugation and filtered through a 0.45μm filter. *GSDMB*$^{-/-}$ HT-29 cells were incubated with viral supernatants for 2d with Polybrene transfection reagent (10μg/mL) and selected in G418 (750 μg/mL).

LDH.—LDH release was analyzed using cyQUANT™ LDH Cytotoxicity Assay as per manufacturer's protocol. Percent cell death was calculated by LDH release = (sample − untreated) / (maximum − untreated) × 100.

PI and SYTOX™ deep red uptake.—1μg/mL PI or 0.5 μg/mL SYTOX™ deep red was added to cells or intact 3D colonoids seeded in 6-well plates. PI was read twice on a SpectraMax i3x Multimode microplate reader at 533/617 (excitation/emission), maximum fluorescence was obtained by using lysed plate. Relative PI uptake was calculated using background (untreated) and maximum fluorescence, and calculated as percent PI uptake = (sample − background) / (maximum − background) × 100. Images for SYTOX were acquired 15 min after dye uptake at 660/682 (excitation/emission) with brightfield overlay using a Keyence Microscope.

EdU staining.—3D colonoids were seeded at a consistent density for all groups and treated with 10μM EdU for 2h incubated at 37°C. Media was removed to add ice-cold PBS to dissolve Matrigel®, followed by harvesting of colonoids into microcentrifuge tubes. Subsequently, protocol outlined by manufacturer for Click-iT EdU Cell Proliferation Kit was followed, with images of stained cells captured at 650/670 (excitation/emission) with brightfield overlay on a Keyence Microscope.

Proliferation assay.—Cells were seeded at a density of 1×10^6 cells/well in 12-well tissue culture plates. Cells were counted each day over a course of 3d by staining with trypan blue 0.4% and counting viable cells using a hemocytometer. Untreated control was set as baseline.

Boyden chamber migration.—Protocol was followed as previously described(Lechuga et al., 2019) using HT-29 cells. Cells were detached from the plate using TrypLE Express solution, resuspended in serum-free media and counted to be added in consistent numbers per upper well chamber of a Transwell® 6.5mm membrane inserts with 0.8μm pores. Membrane inserts were coated with 15μg.cm^2 of collagen I a day prior. Complete media containing 10% FBS as a chemoattractant was added to the lower chamber and cells were allowed to migrate for 12h or 16h at 37°C. Membrane inserts were fixed with methanol and non-migrated cells were removed from the top of the filter using a cotton swab. Cells that remained at bottom of filter, or within membranes, were labeled with ProLong™ Gold Antifade Mountant with DAPI and visualized by a Leica SP8 confocal microscope.

Extracellular matrix adhesion assay.—Protocol was followed as previously described(Lechuga et al., 2019) using HT-29 cells. Cells were detached from the plate, resuspended in complete media, and counted to be added in consistent numbers to each well of a 24-well plate coated with collagen I (coated a day prior). Cells were allowed to adhere for 30 min at 37°C, followed by vacuum aspiration of unattached cells. Wells were then gently washed with HBSS buffer. Remaining cells were fixed with methanol and stained using Crystal Violet Cytotoxicity Kit according to manufacturer's instructions, and visualized using an Axiophot microscope, captured on an Axiocam, and assembled on an Axiovision Release 4.5. Images were processed using Adobe Photoshop, counted using the Image J software on a 20×20mm^2 area.

In vitro wound healing assay.—HT-29 cells were counted and seeded at a density of 1×10^6 into each chamber of a two silicone chamber Culture-Insert 2, placed in a 35mm μ-Dish and incubated overnight at 37°C. Silicone inserts were then removed by sterile forceps, monolayers washed with PBS followed by addition of complete media to dishes. Prior to image acquisition (acquired daily over 3d), old media was removed, monolayers washed with PBS and fresh complete media was added. Images were obtained using an Axiophot microscope, captured on an Axiocam, assembled on an Axiovision Release 4.5, with the distance between leading edges calculated using Image J. The same aforementioned protocol was used with intestinal epithelial organoids, with the additional step of transforming 3D colonoids into 2D monolayers as described above.

Immunolabeling for NM IIA and vinculin.—Protocol was followed as previously described(Lechuga et al., 2019) with HT-29 monolayers cultured on collagen-coated glass coverslips that were mechanically-induced scratch wounded using a 200μl pipette tip, followed by fixation with 4% PFA for 20 min at RT and permeabilization with 0.5% Triton X-100 for 5 min. Scratched monolayers were then blocked with HBSS containing 1% BSA for 1h at RT followed by 1h incubation with primary antibodies and Alexa Fluor-conjugated secondary antibodies diluted in blocking solution; key resource table. Fluorescently labelled cell monolayers were captured on a Leica SP8 confocal microscope and processed using Adobe Photoshop. The same aforementioned protocol was used with intestinal epithelial organoids, with the additional step of transforming 3D colonoids into 2D monolayers as described above.

QUANTIFICATION AND STATISTICAL ANALYSIS

Microarray, scRNA-Seq, RNA-Seq, and GO/pathway enrichment analyses.—For microarray analysis, R package GEOquery(Davis and Meltzer, 2007) was used to download gene array expression data from GSE database accessions GSE20881(Noble et al., 2010), and GSE53306(Zhao et al., 2015). Ambiguous and control probes were filtered out from each data set (presented as log2M). limma R package(Ritchie et al., 2015) was used to fit generalized linear models for each cohort and the empirical Bayes variance moderation method was used to estimate moderate *t* statistics and *P*-values. For scRNA-Seq analysis, 10x Genomics single-cell data were processed as previously described(Parikh et al., 2019). Normalized single-cell expression values were visualized using Seurat package(Butler et al., 2018), with data embeddings generated as previously described(Parikh et al., 2019). Pseudo-bulk analyses were carried out as follows: epithelial cell populations were isolated *in silico*, discarding contaminating immune types, and a pseudo-bulk for each sample was generated by aggregating raw unique molecular identifier counts from selected cellular barcodes for each subpopulation. DESeq2 R package(Love et al., 2014) was used to compute library size factors, normalize data, and perform differential expression analysis using negative binomial Wald's test. Benjamini-Hochberg correction was used to estimate (FDR), and q-values using R package qvalue. For RNA-Seq, sequencing reads generated from the Illumina platform were assessed for quality and trimmed for adapter sequences using TrimGalore! v0.4.2 (Babraham Bioinformatics), a wrapper script for FastQC and cutadapt. Reads that passed quality control were then aligned to the human reference genome (GRCh38) using STAR aligner v2.5.3(Dobin et al., 2013). Alignment for sequences were guided using GENCODE annotation for GRCh38, with aligned reads analyzed for differential expression using Cufflinks v2.2.1(Trapnell et al., 2010), a RNASeq analysis package that reports fragments per kilobase of exon per million fragments mapped (FPKM) for each gene. Differential analysis report was generated using the cuffdiff command performed in a pairwise manner for each group. Differential genes were identified using a significance cutoff of q-value < 0.05. For enriched gene pathway analysis, biological process Gene Ontology (GO) enrichment of significantly upregulated genes in each cluster of UC IECs was performed using the R package clusterProfiler(Yu et al., 2012), with a Benjamini-Hochberg multiple testing adjustment and an FDR cut-off of 0.05, using all expressed/detected genes as background control. Results are visualized as dotplots using clusterProfiler and ggplot2 R packages.

Quantification of Western blot densitometry was performed by pixel density using ImageJ. Data was analyzed using GraphPad Prism 9. Selection of appropriate statistical tests was based on variance and underlying distribution of data. Global effects between groups were first assessed using one-way ANOVA with Dunnett's multiple comparison test. Differences between individual groups were directly compared as indicated in each figure legend, with $P \leq 0.05$ considered significant.

Supplementary Material

Refer to Web version on PubMed Central for supplementary material.

ACKNOWLEDGEMENTS

This work was supported by the NIH: DK091222, DK042191, DK125293 (to TTP), DK108278, DK126702 (to AII), AI141350 (to DWA/TTP), CA214300, DK237304 (to EHH), an institutional MSTP T32 GM007250 (for HCK), and the Biorepository and Morphology/Imaging Cores of DK097948 (Cleveland Digestive Diseases Research Core Center). We acknowledge Claudio Fiocchi, Gail West, Danian Che and Blake Feldman for their supervisory and/or technical support, Asma Nusrat and Chithra Kannachazhath Muraleedharan for their technical assistance with organoid experimentation, and use of the Leica TCS SP8 confocal microscope in the Light Microscopy Imaging Core at CWRU, made available through the Office of Research Infrastructure (NIH-ORIP) shared instrumentation grant S10OD016164.

REFERENCES

Bailey KM, Liu J, 2008. Caveolin-1 Up-regulation during Epithelial to Mesenchymal Transition Is Mediated by Focal Adhesion Kinase. J. Biol. Chem. 283, 13714–13724. 10.1074/jbc.M709329200 [PubMed: 18332144]

Bartolomé RA, Barderas R, Torres S, Fernandez-Aceñero MJ, Mendes M, García-Foncillas J, Lopez-Lucendo M, Casal JI, 2014. Cadherin-17 interacts with α2β1 integrin to regulate cell proliferation and adhesion in colorectal cancer cells causing liver metastasis. Oncogene 33, 1658–1669. 10.1038/onc.2013.117 [PubMed: 23604127]

Bays JL, DeMali KA, 2017. Vinculin in cell–cell and cell–matrix adhesions. Cell. Mol. Life Sci. 74, 2999–3009. 10.1007/s00018-017-2511-3 [PubMed: 28401269]

Broz P, Pelegrín P, Shao F, 2020. The gasdermins, a protein family executing cell death and inflammation. Nat. Rev. Immunol. 20, 143–157. 10.1038/s41577-019-0228-2 [PubMed: 31690840]

Budden KF, Gellatly SL, Wood DLA, Cooper MA, Morrison M, Hugenholtz P, Hansbro PM, 2017. Emerging pathogenic links between microbiota and the gut–lung axis. Nat. Rev. Microbiol. 15, 55–63. 10.1038/nrmicro.2016.142 [PubMed: 27694885]

Bulek K, Zhao J, Liao Y, Rana N, Corridoni D, Antanaviciute A, Chen X, Wang H, Qian W, Miller-Little WA, Swaidani S, Tang F, Willard BB, McCrae K, Kang Z, Dubyak GR, Cominelli F, Simmons A, Pizarro TT, Li X, 2020. Epithelial-derived gasdermin D mediates nonlytic IL-1β release during experimental colitis. J. Clin. Invest. 10.1172/JCI138103. 10.1172/JCI138103

Butler A, Hoffman P, Smibert P, Papalexi E, Satija R, 2018. Integrating single-cell transcriptomic data across different conditions, technologies, and species. Nat. Biotechnol. 36, 411–420. 10.1038/nbt.4096 [PubMed: 29608179]

Çalışkan M, Bochkov YA, Kreiner-Møller E, Bønnelykke K, Stein MM, Du G, Bisgaard H, Jackson DJ, Gern JE, Lemanske RF, Nicolae DL, Ober C, 2013. Rhinovirus Wheezing Illness and Genetic Risk of Childhood-Onset Asthma. N. Engl. J. Med. 368, 1398–1407. 10.1056/NEJMoa1211592 [PubMed: 23534543]

Callahan MJ, Nagymanyoki Z, Bonome T, Johnson ME, Litkouhi B, Sullivan EH, Hirsch MS, Matulonis UA, Liu J, Birrer MJ, Berkowitz RS, Mok SC, 2008. Increased HLA-DMB Expression in the Tumor Epithelium Is Associated with Increased CTL Infiltration and Improved Prognosis in Advanced-Stage Serous Ovarian Cancer. Clin. Cancer Res. 14, 7667–7673. 10.1158/1078-0432.CCR-08-0479 [PubMed: 19047092]

Chao KL, Kulakova L, Herzberg O, 2017. Gene polymorphism linked to increased asthma and IBD risk alters gasdermin-B structure, a sulfatide and phosphoinositide binding protein. Proc. Natl. Acad. Sci. 114, E1128–E1137. 10.1073/pnas.1616783114 [PubMed: 28154144]

Chen P-H, Chen X, He X, 2013. Platelet-derived growth factors and their receptors: Structural and functional perspectives. Biochim. Biophys. Acta BBA - Proteins Proteomics 1834, 2176–2186. 10.1016/j.bbapap.2012.10.015 [PubMed: 23137658]

Chen Q, Shi P, Wang Y, Zou D, Wu X, Wang D, Hu Q, Zou Y, Huang Z, Ren J, Lin Z, Gao X, 2019. GSDMB promotes non-canonical pyroptosis by enhancing caspase-4 activity. J. Mol. Cell Biol. 11, 496–508. 10.1093/jmcb/mjy056 [PubMed: 30321352]

Corridoni D, Antanaviciute A, Gupta T, Fawkner-Corbett D, Aulicino A, Jagielowicz M, Parikh K, Repapi E, Taylor S, Ishikawa D, Hatano R, Yamada T, Xin W, Slawinski H, Bowden R, Napolitani G, Brain O, Morimoto C, Koohy H, Simmons A, 2020. Single-cell atlas of colonic CD8+ T cells in ulcerative colitis. Nat. Med. 26, 1480–1490. 10.1038/s41591-020-1003-4 [PubMed: 32747828]

Cronstein BN, Aune TM, 2020. Methotrexate and its mechanisms of action in inflammatory arthritis. Nat. Rev. Rheumatol. 16, 145–154. 10.1038/s41584-020-0373-9 [PubMed: 32066940]

Das S, Miller M, Beppu AK, Mueller J, McGeough MD, Vuong C, Karta MR, Rosenthal P, Chouiali F, Doherty TA, Kurten RC, Hamid Q, Hoffman HM, Broide DH, 2016. GSDMB induces an asthma phenotype characterized by increased airway responsiveness and remodeling without lung inflammation. Proc. Natl. Acad. Sci. 113, 13132–13137. 10.1073/pnas.1610433113 [PubMed: 27799535]

Davis S, Meltzer PS, 2007. GEOquery: a bridge between the Gene Expression Omnibus (GEO) and BioConductor. Bioinformatics 23, 1846–1847. 10.1093/bioinformatics/btm254 [PubMed: 17496320]

Detjen KM, 2001. Interferon gamma inhibits growth of human pancreatic carcinoma cells via caspase-1 dependent induction of apoptosis. Gut 49, 251–262. 10.1136/gut.49.2.251 [PubMed: 11454803]

Ding J, Wang K, Liu W, She Y, Sun Q, Shi J, Sun H, Wang D-C, Shao F, 2016. Pore-forming activity and structural autoinhibition of the gasdermin family. Nature 535, 111–116. 10.1038/nature18590 [PubMed: 27281216]

Dobin A, Davis CA, Schlesinger F, Drenkow J, Zaleski C, Jha S, Batut P, Chaisson M, Gingeras TR, 2013. STAR: ultrafast universal RNA-seq aligner. Bioinformatics 29, 15–21. 10.1093/bioinformatics/bts635 [PubMed: 23104886]

Evavold CL, Ruan J, Tan Y, Xia S, Wu H, Kagan JC, 2018. The Pore-Forming Protein Gasdermin D Regulates Interleukin-1 Secretion from Living Macrophages. Immunity 48, 35–44.e6. 10.1016/j.immuni.2017.11.013 [PubMed: 29195811]

Fagerberg L, Hallström BM, Oksvold P, Kampf C, Djureinovic D, Odeberg J, Habuka M, Tahmasebpoor S, Danielsson A, Edlund K, Asplund A, Sjöstedt E, Lundberg E, Szigyarto CA-K, Skogs M, Takanen JO, Berling H, Tegel H, Mulder J, Nilsson P, Schwenk JM, Lindskog C, Danielsson F, Mardinoglu A, Sivertsson Å, von Feilitzen K, Forsberg M, Zwahlen M, Olsson I, Navani S, Huss M, Nielsen J, Ponten F, Uhlén M, 2014. Analysis of the Human Tissue-specific Expression by Genome-wide Integration of Transcriptomics and Antibody-based Proteomics. Mol. Cell. Proteomics 13, 397–406. 10.1074/mcp.M113.035600 [PubMed: 24309898]

Graham WV, He W, Marchiando AM, Zha J, Singh G, Li H-S, Biswas A, Ong Ma.L.D.M., Jiang Z-H, Choi W, Zuccola H, Wang Yitang, Griffith J, Wu J, Rosenberg HJ, Wang Yingmin, Snapper SB, Ostrov D, Meredith SC, Miller LW, Turner JR, 2019. Intracellular MLCK1 diversion reverses barrier loss to restore mucosal homeostasis. Nat. Med. 25, 690–700. 10.1038/s41591-019-0393-7 [PubMed: 30936544]

Gurtner GC, Werner S, Barrandon Y, Longaker MT, 2008. Wound repair and regeneration. Nature 453, 314–321. 10.1038/nature07039 [PubMed: 18480812]

Hansen JM, de Jong MF, Wu Q, Zhang L-S, Heisler DB, Alto LT, Alto NM, 2021. Pathogenic ubiquitination of GSDMB inhibits NK cell bactericidal functions. Cell S0092867421005717. 10.1016/j.cell.2021.04.036

Herfarth HH, Kappelman MD, Long MD, Isaacs KL, 2016. Use of Methotrexate in the Treatment of Inflammatory Bowel Diseases: Inflamm. Bowel Dis. 22, 224–233. 10.1097/MIB.0000000000000589

Hu Y-L, Lu S, Szeto KW, Sun J, Wang Y, Lasheras JC, Chien S, 2015. FAK and paxillin dynamics at focal adhesions in the protrusions of migrating cells. Sci. Rep. 4, 6024. 10.1038/srep06024

Hunger-Glaser I, Fan RS, Perez-Salazar E, Rozengurt E, 2004. PDGF and FGF induce focal adhesion kinase (FAK) phosphorylation at Ser-910: Dissociation from Tyr-397 phosphorylation and requirement for ERK activation. J. Cell. Physiol. 200, 213–222. 10.1002/jcp.20018 [PubMed: 15174091]

Jeffes EWB, McCullough JL, Pittelkow MR, McCormick A, Almanzor J, Liu G, Dang M, Voss K, Voss J, Schlotzhauer A, Weinstein GD, 1995. Methotrexate Therapy of Psoriasis: Differential Sensitivity of Proliferating Lymphoid and Epithelial Cells to the Cytotoxic and Growth-Inhibitory Effects of Methotrexate. J. Invest. Dermatol. 104, 183–188. 10.1111/1523-1747.ep12612745 [PubMed: 7829873]

Lechuga S, Amin PH, Wolen AR, Ivanov AI, 2019. Adducins inhibit lung cancer cell migration through mechanisms involving regulation of cell-matrix adhesion and cadherin-11 expression. Biochim. Biophys. Acta BBA - Mol. Cell Res. 1866, 395–408. 10.1016/j.bbamcr.2018.10.001

Leoni G, Neumann P-A, Sumagin R, Denning TL, Nusrat A, 2015. Wound repair: role of immune–epithelial interactions. Mucosal Immunol. 8, 959–968. 10.1038/mi.2015.63 [PubMed: 26174765]

Li L, Li Y, Bai Y, 2020. Role of GSDMB in Pyroptosis and Cancer. Cancer Manag. Res. Volume 12, 3033–3043. 10.2147/CMAR.S246948 [PubMed: 32431546]

Li X, Christenson SA, Modena B, Li H, Busse WW, Castro M, Denlinger LC, Erzurum SC, Fahy JV, Gaston B, Hastie AT, Israel E, Jarjour NN, Levy BD, Moore WC, Woodruff PG, Kaminski N, Wenzel SE, Bleecker ER, Meyers DA, 2020. Genetic analyses identify GSDMB associated with asthma severity, exacerbations, and antiviral pathways. J. Allergy Clin. Immunol. S009167492031112X. 10.1016/j.jaci.2020.07.030

Liu W, Liang Y, Chan Q, Jiang L, Dong J, 2019. CX3CL1 promotes lung cancer cell migration and invasion via the Src/focal adhesion kinase signaling pathway. Oncol. Rep. 10.3892/or.2019.6957

Love MI, Huber W, Anders S, 2014. Moderated estimation of fold change and dispersion for RNA-seq data with DESeq2. Genome Biol. 15, 550. 10.1186/s13059-014-0550-8 [PubMed: 25516281]

Ma Z, Lou S, Jiang Z, 2020. PHLDA2 regulates EMT and autophagy in colorectal cancer via the PI3K/AKT signaling pathway. Aging 12, 7985–8000. 10.18632/aging.103117 [PubMed: 32385195]

McCloskey P, Fridell Y-W, Attar E, Villa J, Jin Y, Varnum B, Liu ET, 1997. GAS6 Mediates Adhesion of Cells Expressing the Receptor Tyrosine Kinase Axl. J. Biol. Chem. 272, 23285–23291. 10.1074/jbc.272.37.23285 [PubMed: 9287338]

McLean GW, Carragher NO, Avizienyte E, Evans J, Brunton VG, Frame MC, 2005. The role of focal-adhesion kinase in cancer — a new therapeutic opportunity. Nat. Rev. Cancer 5, 505–515. 10.1038/nrc1647 [PubMed: 16069815]

Miyoshi H, Stappenbeck TS, 2013. In vitro expansion and genetic modification of gastrointestinal stem cells in spheroid culture. Nat. Protoc. 8, 2471–2482. 10.1038/nprot.2013.153 [PubMed: 24232249]

Moffatt MF, Kabesch M, Liang L, Dixon AL, Strachan D, Heath S, Depner M, von Berg A, Bufe A, Rietschel E, Heinzmann A, Simma B, Frischer T, Willis-Owen SAG, Wong KCC, Illig T, Vogelberg C, Weiland SK, von Mutius E, Abecasis GR, Farrall M, Gut IG, Lathrop GM, Cookson WOC, 2007. Genetic variants regulating ORMDL3 expression contribute to the risk of childhood asthma. Nature 448, 470–473. 10.1038/nature06014 [PubMed: 17611496]

Munir J, Van Ngu T, Na Ayudthaya PD, Ryu S, 2020. Downregulation of glypican-4 facilitates breast cancer progression by inducing cell migration and proliferation. Biochem. Biophys. Res. Commun. 526, 91–97. 10.1016/j.bbrc.2020.03.064 [PubMed: 32199612]

Noble CL, Abbas AR, Lees CW, Cornelius J, Toy K, Modrusan Z, Clark HF, Arnott ID, Penman ID, Satsangi J, Diehl L, 2010. Characterization of intestinal gene expression profiles in Crohn's disease by genome-wide microarray analysis: Inflamm. Bowel Dis. 16, 1717–1728. 10.1002/ibd.21263

Odenwald MA, Turner JR, 2017. The intestinal epithelial barrier: a therapeutic target? Nat. Rev. Gastroenterol. Hepatol. 14, 9–21. 10.1038/nrgastro.2016.169 [PubMed: 27848962]

Parikh K, Antanaviciute A, Fawkner-Corbett D, Jagielowicz M, Aulicino A, Lagerholm C, Davis S, Kinchen J, Chen HH, Alham NK, Ashley N, Johnson E, Hublitz P, Bao L, Lukomska J, Andev RS, Björklund E, Kessler BM, Fischer R, Goldin R, Koohy H, Simmons A, 2019. Colonic epithelial cell diversity in health and inflammatory bowel disease. Nature 567, 49–55. 10.1038/s41586-019-0992-y [PubMed: 30814735]

Pasello M, Manara MC, Scotlandi K, 2018. CD99 at the crossroads of physiology and pathology. J. Cell Commun. Signal. 12, 55–68. 10.1007/s12079-017-0445-z [PubMed: 29305692]

Pastorelli L, Garg RR, Hoang SB, Spina L, Mattioli B, Scarpa M, Fiocchi C, Vecchi M, Pizarro TT, 2010. Epithelial-derived IL-33 and its receptor ST2 are dysregulated in ulcerative colitis and in experimental Th1/Th2 driven enteritis. Proc. Natl. Acad. Sci. 107, 8017–8022. 10.1073/pnas.0912678107 [PubMed: 20385815]

Pouillon L, Travis S, Bossuyt P, Danese S, Peyrin-Biroulet L, 2020. Head-to-head trials in inflammatory bowel disease: past, present and future. Nat. Rev. Gastroenterol. Hepatol. 17, 365–376. 10.1038/s41575-020-0293-9 [PubMed: 32303700]

Ran FA, Hsu PD, Wright J, Agarwala V, Scott DA, Zhang F, 2013. Genome engineering using the CRISPR-Cas9 system. Nat. Protoc. 8, 2281–2308. 10.1038/nprot.2013.143 [PubMed: 24157548]

Rashmi, More SK, Wang Q, Vomhof- DeKrey EE, Porter JE, Basson MD, 2021. ZINC40099027 activates human focal adhesion kinase by accelerating the enzymatic activity of the FAK kinase domain. Pharmacol. Res. Perspect. 9. 10.1002/prp2.737

Reed M, Luissint A-C, Azcutia V, Fan S, O'Leary MN, Quiros M, Brazil J, Nusrat A, Parkos CA, 2019. Epithelial CD47 is critical for mucosal repair in the murine intestine in vivo. Nat. Commun. 10, 5004. 10.1038/s41467-019-12968-y [PubMed: 31676794]

Ridley AJ, 2003. Cell Migration: Integrating Signals from Front to Back. Science 302, 1704–1709. 10.1126/science.1092053 [PubMed: 14657486]

Ritchie ME, Phipson B, Wu D, Hu Y, Law CW, Shi W, Smyth GK, 2015. limma powers differential expression analyses for RNA-sequencing and microarray studies. Nucleic Acids Res. 43, e47–e47. 10.1093/nar/gkv007 [PubMed: 25605792]

Rizzo P, Novelli R, Rota C, Gagliardini E, Ruggiero B, Rottoli D, Benigni A, Remuzzi G, 2017. The Role of Angiotensin II in Parietal Epithelial Cell Proliferation and Crescent Formation in Glomerular Diseases. Am. J. Pathol. 187, 2441–2450. 10.1016/j.ajpath.2017.07.004 [PubMed: 28807596]

Rossi M, Bucci G, Rizzotto D, Bordo D, Marzi MJ, Puppo M, Flinois A, Spadaro D, Citi S, Emionite L, Cilli M, Nicassio F, Inga A, Briata P, Gherzi R, 2019. LncRNA EPR controls epithelial proliferation by coordinating Cdkn1a transcription and mRNA decay response to TGF-β. Nat. Commun. 10, 1969. 10.1038/s41467-019-09754-1 [PubMed: 31036808]

Saeki N, Usui T, Aoyagi K, Kim DH, Sato M, Mabuchi T, Yanagihara K, Ogawa K, Sakamoto H, Yoshida T, Sasaki H, 2009. Distinctive expression and function of four *GSDM* family genes (*GSDMA-D*) in normal and malignant upper gastrointestinal epithelium. Genes. Chromosomes Cancer 48, 261–271. 10.1002/gcc.20636 [PubMed: 19051310]

Sarvestani SK, Signs SA, Lefebvre V, Mack S, Ni Y, Morton A, Chan ER, Li X, Fox P, Ting A, Kalady MF, Cruise M, Ashburn J, Stiene J, Lai W, Liska D, Xiang S, Huang EH, 2018. Cancer-predicting transcriptomic and epigenetic signatures revealed for ulcerative colitis in patient-derived epithelial organoids. Oncotarget 9, 28717–28730. 10.18632/oncotarget.25617 [PubMed: 29983891]

Schaller MD, 2010. Cellular functions of FAK kinases: insight into molecular mechanisms and novel functions. J. Cell Sci. 123, 1007–1013. 10.1242/jcs.045112 [PubMed: 20332118]

Schneider CA, Rasband WS, Eliceiri KW, 2012. NIH Image to ImageJ: 25 years of image analysis. Nat. Methods 9, 671–675. 10.1038/nmeth.2089 [PubMed: 22930834]

Shi J, Zhao Y, Wang K, Shi X, Wang Y, Huang H, Zhuang Y, Cai T, Wang F, Shao F, 2015. Cleavage of GSDMD by inflammatory caspases determines pyroptotic cell death. Nature 526, 660–665. 10.1038/nature15514 [PubMed: 26375003]

Singh J, Sharma K, Frost EE, Pillai PP, 2019. Role of PDGF-A-Activated ERK Signaling Mediated FAK-Paxillin Interaction in Oligodendrocyte Progenitor Cell Migration. J. Mol. Neurosci. 67, 564–573. 10.1007/s12031-019-1260-1 [PubMed: 30649683]

Stein MM, 2018. A decade of research on the 17q12–21 asthma locus: Piecing together the puzzle. J ALLERGY CLIN IMMUNOL 142, 19.

Tang L, Lu C, Zheng G, Burgering BM, 2020. Emerging insights on the role of gasdermins in infection and inflammatory diseases. Clin. Transl. Immunol. 9. 10.1002/cti2.1186

The International IBD Genetics Consortium (IIBDGC), Jostins L, Ripke S, Weersma RK, Duerr RH, McGovern DP, Hui KY, Lee JC, Philip Schumm L, Sharma Y, Anderson CA, Essers J, Mitrovic M, Ning K, Cleynen I, Theatre E, Spain SL, Raychaudhuri S, Goyette P, Wei Z, Abraham C, Achkar J-P, Ahmad T, Amininejad L, Ananthakrishnan AN, Andersen V, Andrews JM, Baidoo L, Balschun T, Bampton PA, Bitton A, Boucher G, Brand S, Büning C, Cohain A, Cichon S, D'Amato M, De Jong D, Devaney KL, Dubinsky M, Edwards C, Ellinghaus D, Ferguson LR, Franchimont D, Fransen K, Gearry R, Georges M, Gieger C, Glas J, Haritunians T, Hart A, Hawkey C, Hedl M, Hu X, Karlsen TH, Kupcinskas L, Kugathasan S, Latiano A, Laukens D, Lawrance IC, Lees CW, Louis E, Mahy G, Mansfield J, Morgan AR, Mowat C, Newman W, Palmieri O, Ponsioen CY, Potocnik U, Prescott NJ, Regueiro M, Rotter JI, Russell RK, Sanderson JD, Sans M, Satsangi J, Schreiber S, Simms LA, Sventoraityte J, Targan SR, Taylor KD, Tremelling M, Verspaget HW, De Vos M, Wijmenga C, Wilson DC, Winkelmann J, Xavier RJ, Zeissig S, Zhang B, Zhang CK, Zhao H, Silverberg MS, Annese V, Hakonarson H, Brant SR, Radford-Smith G, Mathew CG, Rioux JD, Schadt EE, Daly MJ, Franke A, Parkes M, Vermeire S, Barrett JC, Cho JH, 2012. Host–microbe interactions have shaped the genetic architecture of inflammatory bowel disease. Nature 491, 119–124. 10.1038/nature11582 [PubMed: 23128233]

Trapnell C, Williams BA, Pertea G, Mortazavi A, Kwan G, van Baren MJ, Salzberg SL, Wold BJ, Pachter L, 2010. Transcript assembly and quantification by RNA-Seq reveals unannotated transcripts and isoform switching during cell differentiation. Nat. Biotechnol. 28, 511–515. 10.1038/nbt.1621 [PubMed: 20436464]

Uchiyama Y, Sakaguchi M, Terabayashi T, Inenaga T, Inoue S, Kobayashi C, Oshima N, Kiyonari H, Nakagata N, Sato Y, Sekiguchi K, Miki H, Araki E, Fujimura S, Tanaka SS, Nishinakamura R, 2010. Kif26b, a kinesin family gene, regulates adhesion of the embryonic kidney mesenchyme. Proc. Natl. Acad. Sci. 107, 9240–9245. 10.1073/pnas.0913748107 [PubMed: 20439720]

Winship A, Van Sinderen M, Heffernan-Marks A, Dimitriadis E, 2017. Chondroitin sulfate proteoglycan protein is stimulated by interleukin 11 and promotes endometrial epithelial cancer cell proliferation and migration. Int. J. Oncol. 50, 798–804. 10.3892/ijo.2017.3848 [PubMed: 28098860]

Xu F, Shangguan X, Pan J, Yue Z, Shen K, Ji Y, Zhang W, Zhu Y, Sha J, Wang Y, Fan L, Dong B, Wang Q, Xue W, 2021. HOXD13 suppresses prostate cancer metastasis and BMP4 - induced epithelial- mesenchymal transition by inhibiting SMAD1. Int. J. Cancer 148, 3060–3070. 10.1002/ijc.33494 [PubMed: 33521930]

Xu J, Lamouille S, Derynck R, 2009. TGF-β-induced epithelial to mesenchymal transition. Cell Res. 19, 156–172. 10.1038/cr.2009.5 [PubMed: 19153598]

Yu G, Wang L-G, Han Y, He Q-Y, 2012. clusterProfiler: an R Package for Comparing Biological Themes Among Gene Clusters. OMICS J. Integr. Biol. 16, 284–287. 10.1089/omi.2011.0118

Yu J, Liu D, Sun X, Yang K, Yao J, Cheng C, Wang C, Zheng J, 2019. CDX2 inhibits the proliferation and tumor formation of colon cancer cells by suppressing Wnt/β-catenin signaling via transactivation of GSK-3β and Axin2 expression. Cell Death Dis. 10, 26. 10.1038/s41419-018-1263-9 [PubMed: 30631044]

Yu J, Shen W, Gao B, Xu J, Gong B, 2020. Metastasis suppressor 1 acts as a tumor suppressor by inhibiting epithelial-to-mesenchymal transition in triple-negative breast cancer. Int. J. Biol. Markers 35, 74–81. 10.1177/1724600820905114

Zhao X, Fan J, Zhi F, Li A, Li C, Berger AE, Boorgula MP, Barkataki S, Courneya J-P, Chen Y, Barnes KC, Cheadle C, 2015. Mobilization of epithelial mesenchymal transition genes distinguishes active from inactive lesional tissue in patients with ulcerative colitis. Hum. Mol. Genet. 24, 4615–4624. 10.1093/hmg/ddv192 [PubMed: 26034135]

Zhou W-J, Geng ZH, Chi S, Zhang W, Niu X-F, Lan S-J, Ma L, Yang X, Wang L-J, Ding Y-Q, Geng J-G, 2011. Slit-Robo signaling induces malignant transformation through Hakai-mediated E-cadherin degradation during colorectal epithelial cell carcinogenesis. Cell Res. 21, 609–626. 10.1038/cr.2011.17 [PubMed: 21283129]

Zhou Z, He H, Wang K, Shi X, Wang Yupeng, Su, Wang Yao, Li D, Liu W, Zhang Y, Shen Lianjun, Han W, Shen Lin, Ding J, Shao F, 2020. Granzyme A from cytotoxic lymphocytes cleaves GSDMB to trigger pyroptosis in target cells. Science 368, eaaz7548. 10.1126/science.aaz7548 [PubMed: 32299851]

Highlights

- GSDMB is increased in IBD vs. healthy patients and localizes to the gut epithelium.
- GSDMB promotes epithelial restitution and repair independent of pyroptosis.
- Carriage of IBD-associated mutant GSDMB confers dysregulated epithelial function.
- PDGF-A-mediated FAK phosphorylation is regulated by GSDMB.

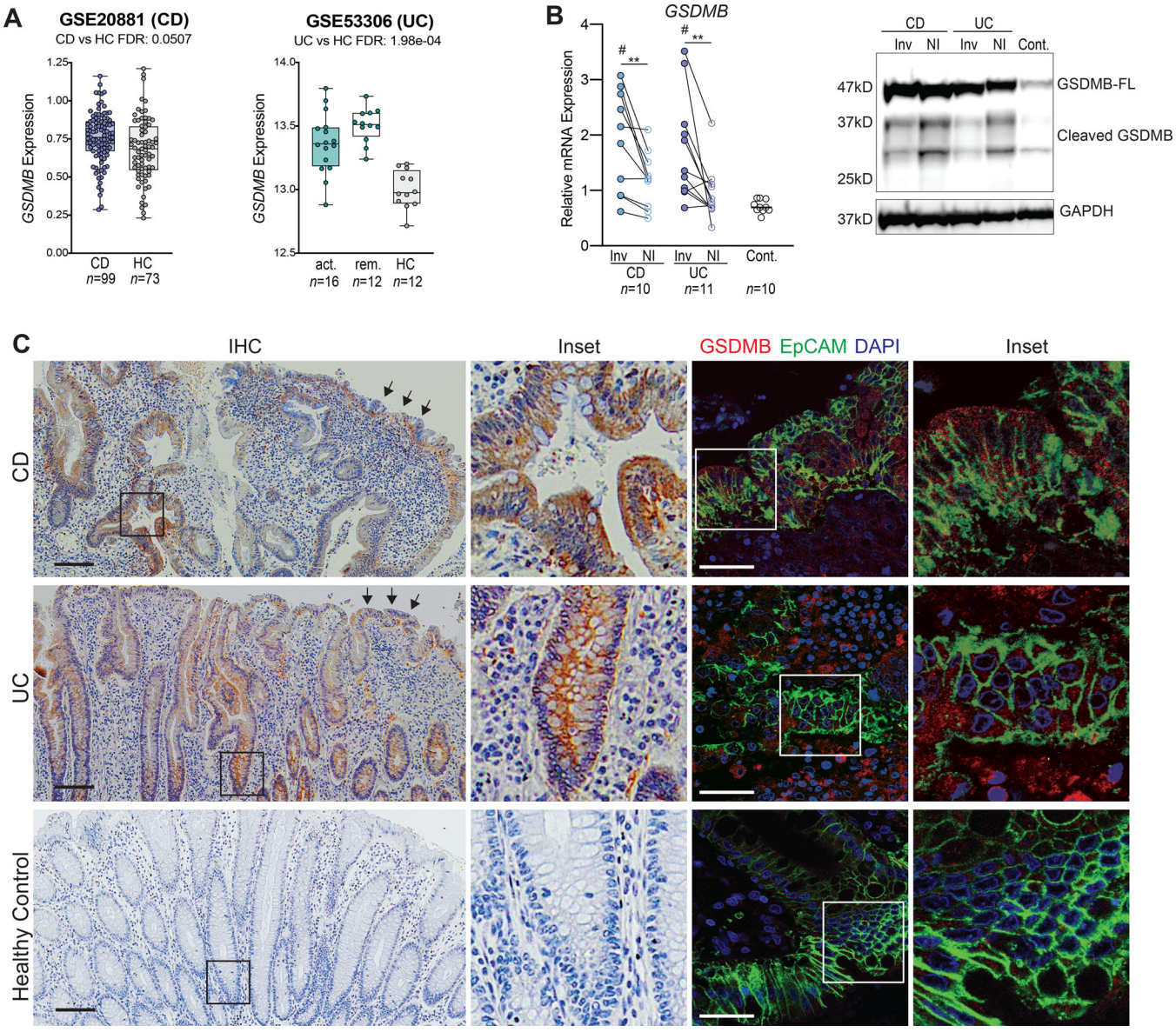

Figure 1. Increased GSDMB in inflamed lesions of IBD patients vs. healthy controls.

(A) Analysis of 2 different IBD gene array expression datasets (GSE database system) derived from intestinal mucosal biopsies of CD and UC patients, during active disease (act.) and remission (rem.), compared to healthy controls (HC). Data displayed as box plots (25th, 50th, and 75th quantiles shown), with differences expressed as FDR between IBD patients and HC.

(B) Relative *GSDMB* in involved (Inv) and non-involved (NI) gut mucosal biopsies from CD and UC patients, shown as fold-difference vs. healthy controls (Cont., set arbitrarily as 1) (*left*), and representative Western blot (*right*) of corresponding full-length (FL) and cleaved GSDMB proteins, with GAPDH used as loading control (n=4). See also Figure S1C.

(C) Representative IHC for GSDMB (*left*), highlighting expression in IEC and single-layer restituting epithelium of IBD patients (*arrows*), with confocal images (*right*) co-localizing

EpCAM (*green*) and GSDMB (*red*) within and at plasma membranes of IECs (*arrowheads*) (n=4). Scale bar = 100μm.

Data presented as mean ± SEM, non-significant (ns) $P \geq 0.01$; $^{**}P<0.01$ by paired Student's t-test and $^{\#}P<0.05$ vs. Cont. by one-way ANOVA with multiple comparisons. All experiments were repeated three times and yielded consistent results.

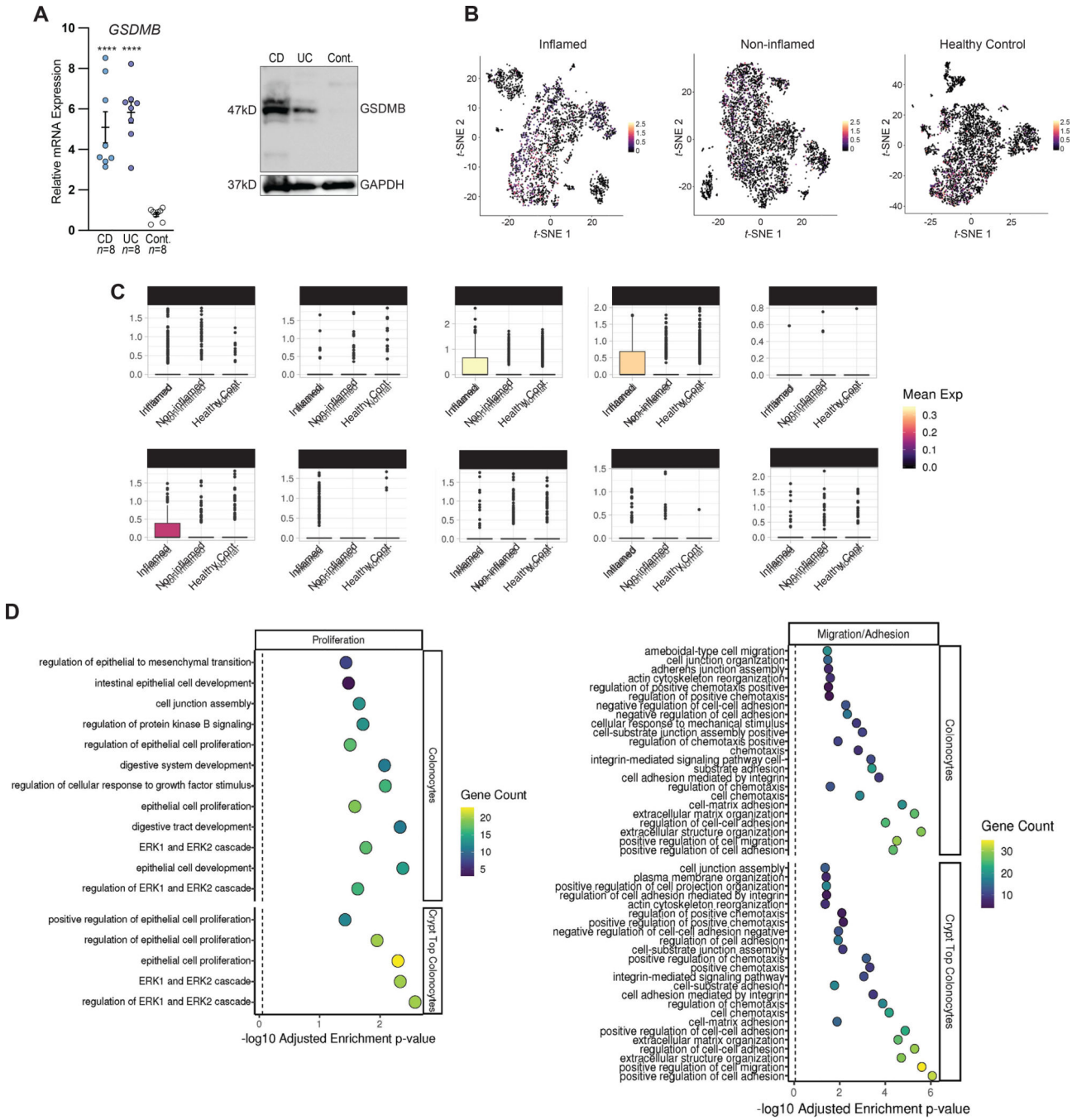

Figure 2. GSDMB is increased and localizes to IECs from IBD patients.

(A) Relative *GSDMB* in freshly isolated IECs from CD and UC patients shown as fold-difference vs. Cont. (set arbitrarily as 1) (*left*), and representative Western blot (*right*) of corresponding GSDMB protein with GAPDH used as loading control (n=4).

(B and C) t-SNE plots after scRNA-Seq of colonic IECs depicting expression and distribution of *GSDMB* mapped to referenced IEC clusters (Figure S1C), with bar plots demonstrating *GSDMB* in epithelial subpopulations of inflamed/non-inflamed UC patients and healthy control (n=3).

(D) Dotplots summarizing selected enriched Gene Ontology biological processes in UC single cell colonocytes (*top*) and crypt top colonocytes (*lower*). Dots are colored by number of significantly upregulated genes within each gene set (<1% FDR); dashed lines indicate adjusted *P*-value threshold of 0.01. Processes are grouped by proliferation- (*left*) and migration/adhesion- (*right*) related functions.

Data presented as mean ± SEM, ns $P \geq 0.01$; **** $P < 0.0001$ vs. Cont. by one-way ANOVA with multiple comparisons. DESeq2 R package was used to compute library size factors, normalize data and perform differential expression analysis using negative binomial Wald's test. For dotplots, Benjamini-Hochberg multiple testing adjustment and FDR cut-off of 0.05 was employed, using all expressed/detected genes as background control. Experiments in (A) were repeated four times and yielded consistent results.

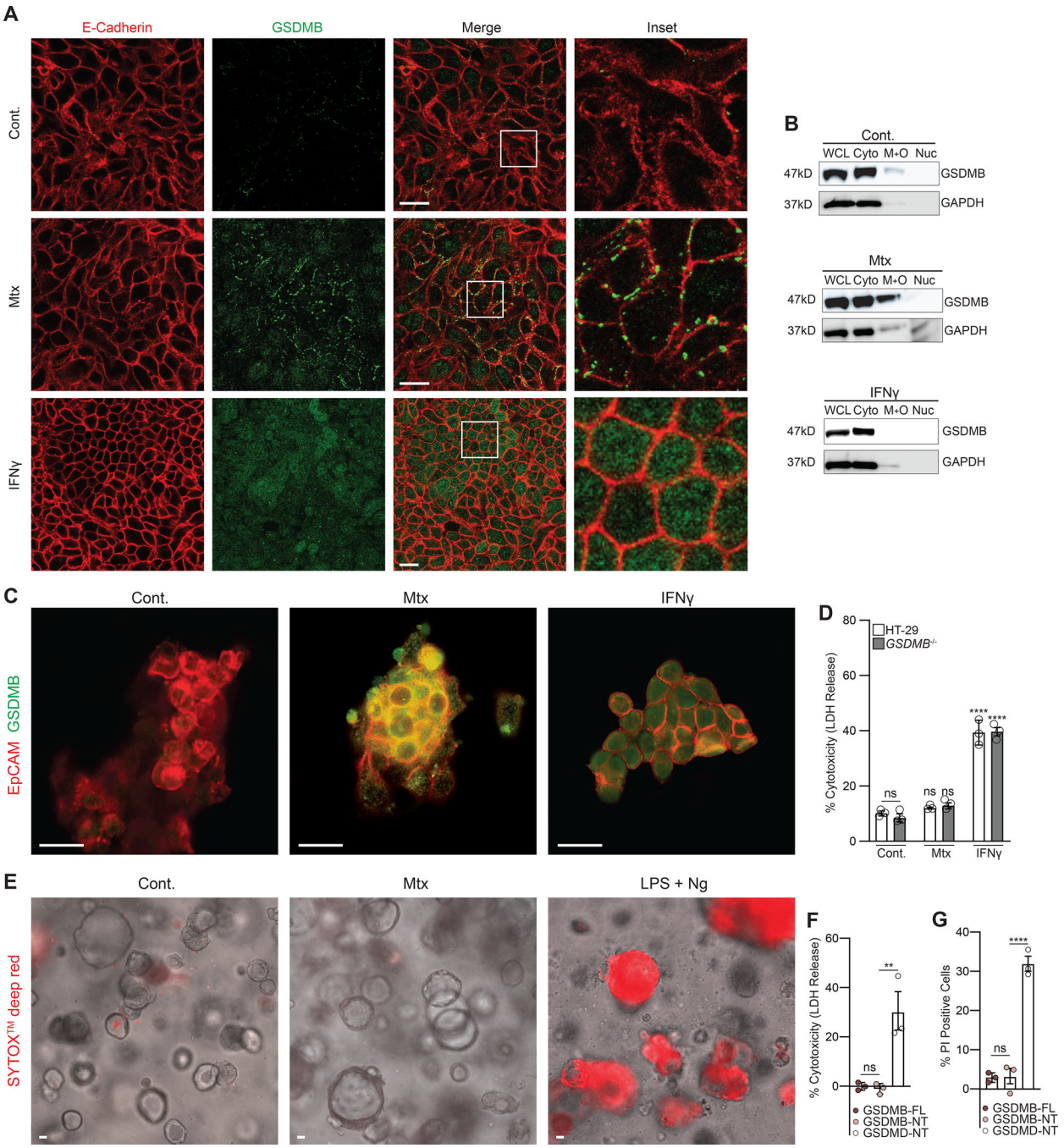

Figure 3. GSDMB translocates to the plasma membrane after *in vitro* stimulation with Mtx, but does not induce canonical pyroptosis.

(A) Representative confocal images of HT-29 cells co-localizing E-cadherin (*red*) and GSDMB (*green*) to plasma membrane (*arrowheads*) after methotrexate (Mtx) (*middle*) or accumulating intracellularly after IFNγ stimulation (*lower*) (n=3).

(B) Representative Western blot showing subcellular fractionation of GSDMB within WCL (whole cell lysate), Cyto (cytoplasmic), M+O (membrane and organelle) and Nuc (nuclear) compartments in HT-29 cells after either Mtx or IFNγ stimulation (n=4).

(C) Representative confocal images of 2D monolayers transformed from colonic epithelial organoids co-localizing EpCAM (*red*) and GSDMB (*green*) to plasma membrane (yellow, *arrowheads*) after Mtx (*middle*) or accumulating intracellularly after IFNγ stimulation (*right*) (n=3).

(D) Supernatants from *GSDMB*$^{-/-}$ (knockout) vs. WT HT-29 cells +/− Mtx, or IFNγ, analyzed for LDH release (normalized as total % cytotoxicity) (n=3).

(E) Representative brightfield and fluorescent images of SYTOX™ deep red uptake in colonic epithelial organoids after Mtx (*middle*) or LPS+Ng (nigericin) (positive control) (*right*) (n=3).

(F and G) HEK293T cells transfected with constructs overexpressing either FL or N-terminal fragment (NT) GSDMB, with GSDMD-NT serving as positive control, and analyzed for LDH release and % PI uptake. See also Figure S4D.

Scale bar = 20μm. Data presented as mean ± SEM, ns $P \geq 0.01$; *$P<0.05$, **$P<0.01$, ***$P<0.001$, ****$P<0.0001$ vs. Cont. (unless otherwise noted) by one-way ANOVA with multiple comparisons. All experiments were repeated three times and yielded consistent results.

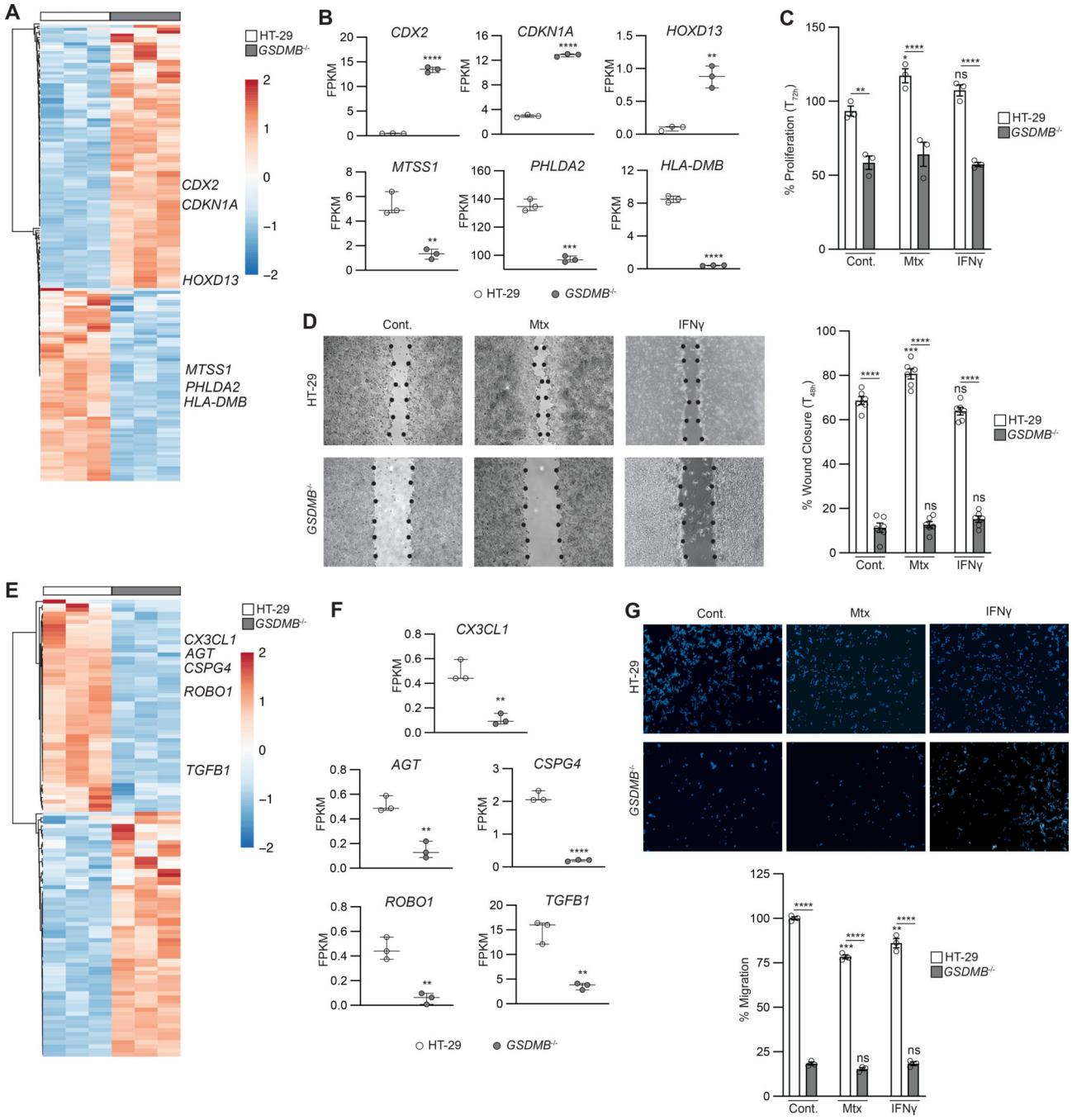

Figure 4. Epithelial-derived GSDMB regulates cell proliferation and migration.

(A and B) Heatmap of differentially expressed genes related to proliferation from RNA-Seq of *GSDMB*$^{-/-}$ vs. WT HT-29 cells. Rows are centered for each gene with unit variance scaling applied, gene clustering by correlation distance and average linkage. Comparative expression of top six proliferation-associated genes expressed as FPKM for each replicate. (C and D) *GSDMB*$^{-/-}$ vs. WT HT-29 cells +/− either Mtx or IFNγ analyzed for proliferation and wound closure (representative scratch assay shown) (n=3).

(E and F) Heatmap of differentially expressed genes related to migration from RNA-Seq of *GSDMB*$^{-/-}$ vs. WT HT-29 cells. Rows are centered for each gene with unit variance scaling applied, gene clustering by correlation distance and average linkage. Comparative expression of top five migration-associated genes expressed as FPKM for each replicate. (G) *GSDMB*$^{-/-}$ vs. WT HT-29 cells +/− either Mtx or IFNγ analyzed for Boyden chamber migration (stained with DAPI) (n=3).

Significance for gene set enrichment analysis was determined using Cuffdiff, with a cutoff of P<0.05 after Benjamini Hochberg correction for multiple testing. Data presented as mean ± SEM, ns P≥ 0.01; **P<0.01, ***P<0.001, ****P<0.0001 vs. Cont. (unless otherwise noted) by Student's t-test and one-way ANOVA with multiple comparisons. All experiments were repeated three times and yielded consistent results.

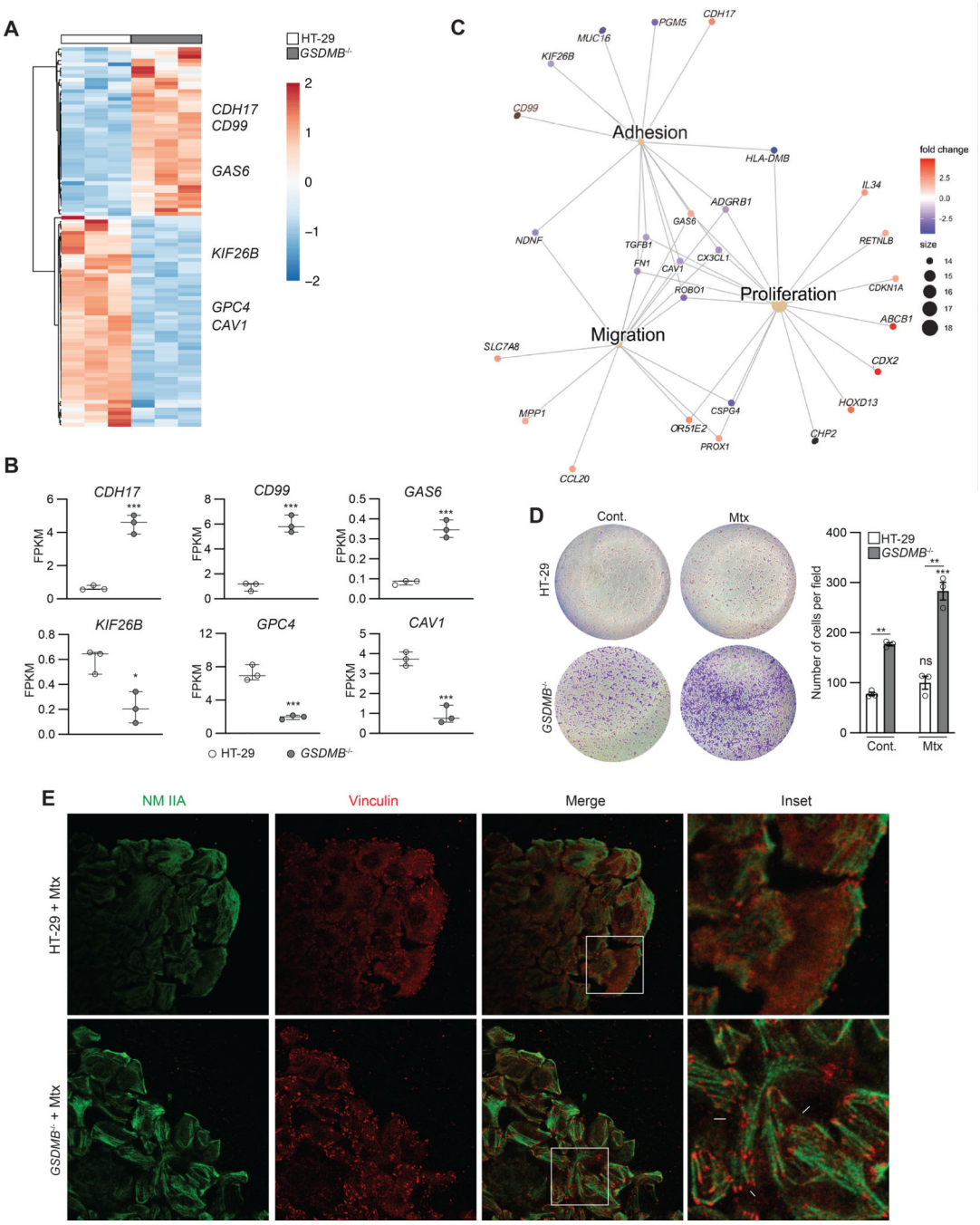

Figure 5. Lack of GSDMB confers hyper-adhesive phenotype in IECs.

(A and B) Heatmap of differentially expressed genes related to adhesion from RNA-Seq of *GSDMB*$^{-/-}$ vs. WT HT-29 cells. Rows are centered for each gene with unit variance scaling applied, gene clustering by correlation distance and average linkage. Comparative expression of top six adhesion-associated genes expressed as FPKM for each replicate. (C) Network analysis generated with Enrichplot and ClusterProfiler demonstrating relative relationship among expressed genes with log2(F) > 2 and central nodes of proliferation, migration and adhesion.

(D) *GSDMB*$^{-/-}$ vs. WT HT-29 cells +/− Mtx analyzed for extracellular matrix adhesion (stained with crystal violet) (n=3).

(E) Representative confocal images of activated WT and *GSDMB*$^{-/-}$ cells stained for NM IIA (*green*) and vinculin (*red*), highlighting increased formation of vinculin-based focal adhesions (*arrows*) and actomyosin stress fibers (n=3). Scale bar = 20μm.

Significance for gene set enrichment analysis was determined using Cuffdiff, with a cutoff of P<0.05 after Benjamini Hochberg correction for multiple testing. Data presented as mean ± SEM, ns P≥ 0.01; **P<0.01, ***P<0.001, ****P<0.0001 vs. Cont. (unless otherwise noted) by Student's t-test and one-way ANOVA with multiple comparisons. All experiments were repeated three times and yielded consistent results.

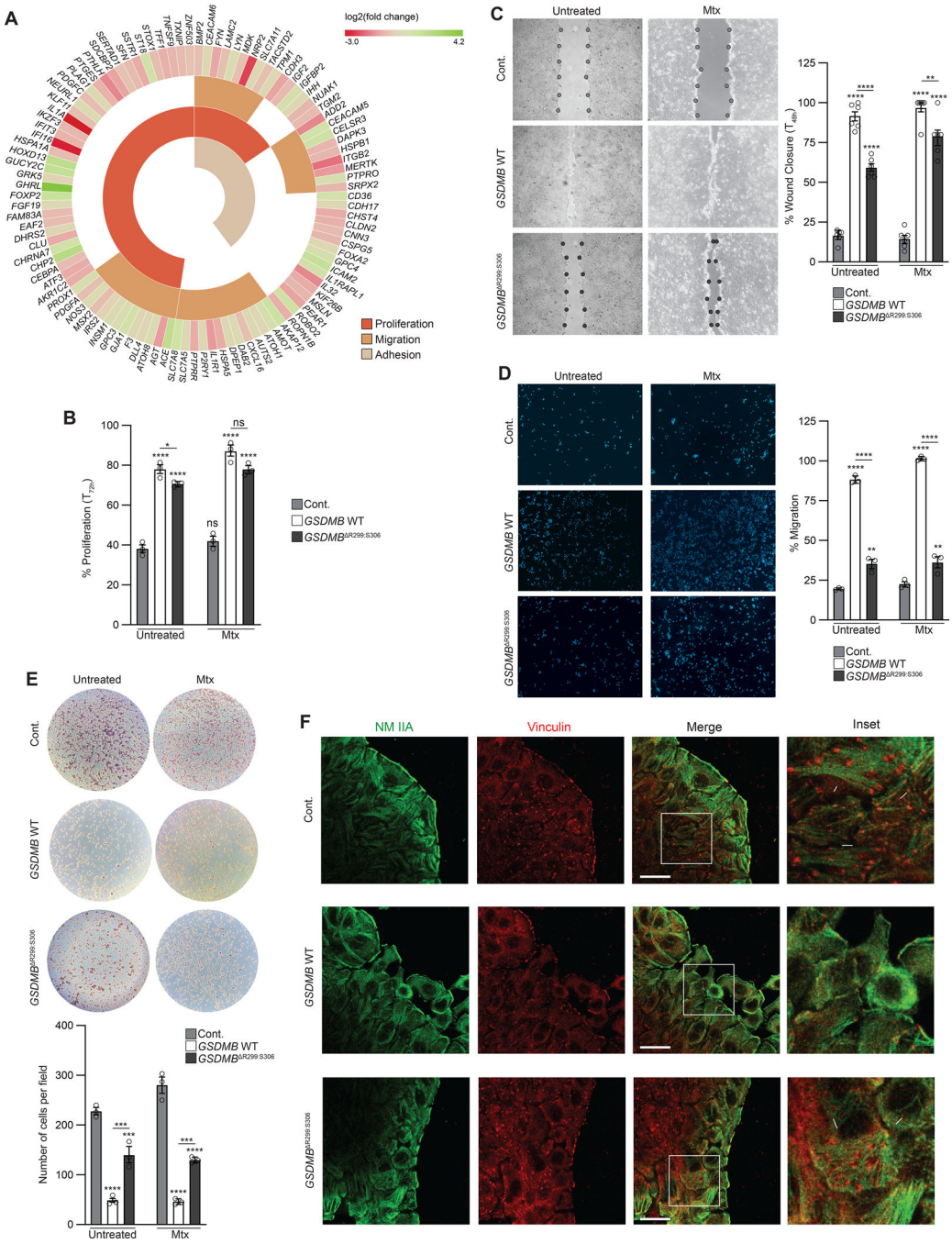

Figure 6. IBD-associated *GSDMB* SNPs (Gly299Arg, Pro306Ser) diminish *in vitro* IEC wound healing functions.

(A) Circos plot comparing differentially expressed genes by RNA-Seq after rescue of *GSDMB*$^{-/-}$ HT-29 IECs with either *GSDMB* WT- or *GSDMB*$^{\Delta R299:S306}$-encoded protein, highlighting molecules related to proliferation, migration and adhesion (FDR adjusted *P*-value <0.05).

(B - E) *GSDMB* WT vs. *GSDMB*$^{\Delta R299:S306}$ rescued HT-29 IECs were subjected to *in vitro* functional assays, including proliferation, wound closure (representative scratch assay shown), Boyden chamber migration (stained with DAPI), and extracellular matrix adhesion

(stained with crystal violet), with *GSDMB*$^{-/-}$ IECs transfected with empty vector serving as control (Cont.) (n=3).

(F) Representative confocal images of experimental groups stained for NM IIA (*green*) and vinculin (*red*), highlighting increased formation of vinculin-based focal adhesions (*arrows*) and actomyosin stress fibers (n=3). Scale bar = 20μm.

Data presented as mean ± SEM, ns $P \geq 0.01$; *$P<0.05$, **$P<0.01$, ***$P<0.001$, ****$P<0.0001$ vs. Cont. (unless otherwise noted) by one-way ANOVA with multiple comparisons. All experiments were repeated three times and yielded consistent results.

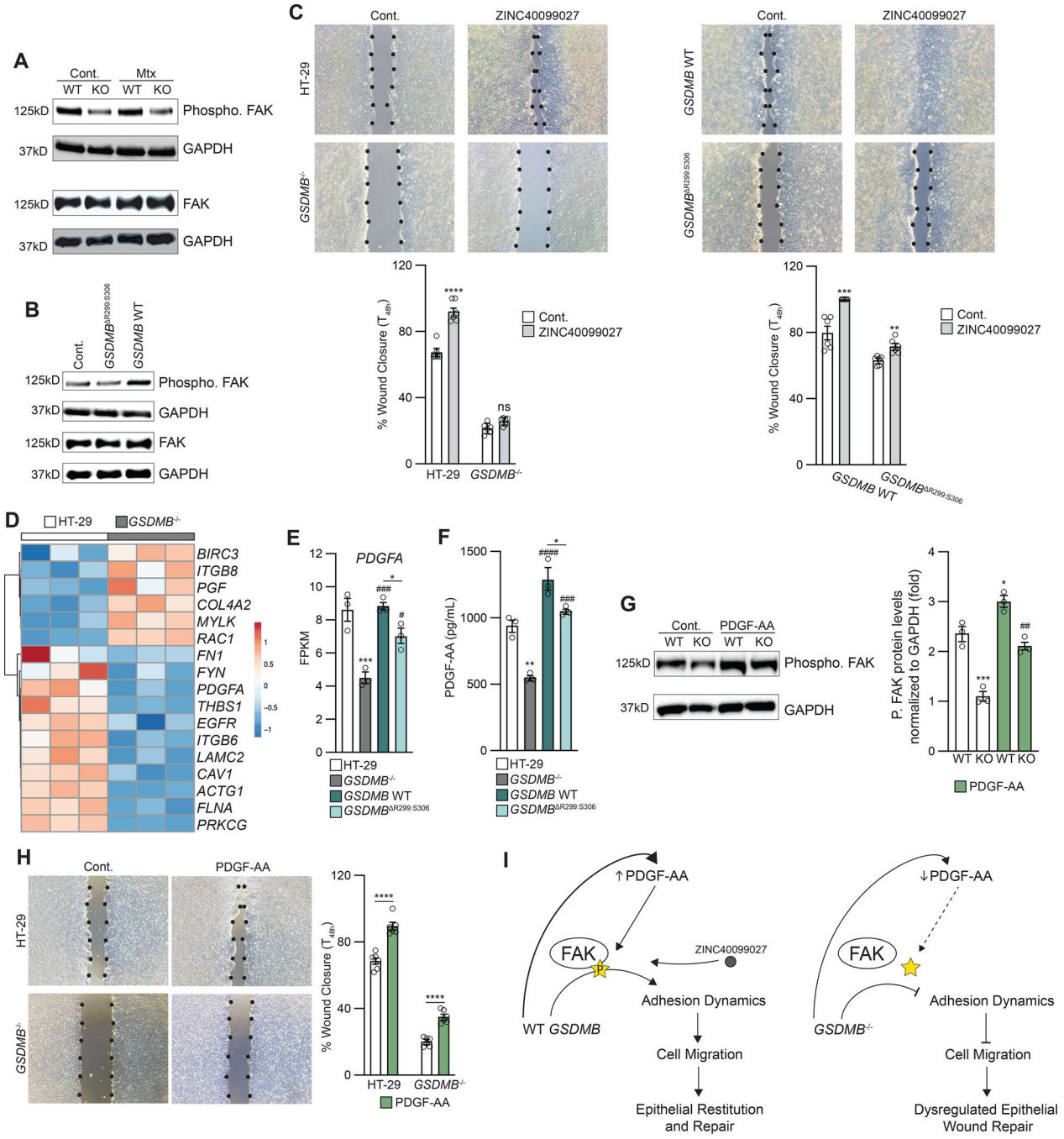

Figure 7. GSDMB promotes *in vitro* epithelial wound closure by phosphorylation of FAK via *PDGFA*.

(A and B) Representative Western blot of lysates from experimental groups probed for phospho, and total FAK, with GAPDH as loading control (n=3).

(C) WT HT-29, *GSDMB*$^{-/-}$, *GSDMB* WT, and *GSDMB*$^{\Delta R299:S306}$ rescued cells +/− ZINC40099027, analyzed for *in vitro* wound closure (representative scratch assay shown) (n=3).

(D) Heatmap of differentially expressed genes related to FAK-associated functions from RNA-Seq of *GSDMB*$^{-/-}$ vs. WT HT-29 cells. Rows are centered for each gene with unit variance scaling applied, gene clustering by correlation distance and average linkage.
(E) Comparative expression of *PDGFA* in experimental groups expressed as FPKM for each replicate.
(F) Quantification of PDGF-AA protein in experimental groups (n=3).
(G) Representative Western blot of WT HT-29 vs. *GSDMB*$^{-/-}$ +/− PDGF-AA probed for phospho FAK; GAPDH used as loading control (*left*), with relative densitometric values (*right*) (n=3).
(H) WT HT-29 vs. *GSDMB*$^{-/-}$ +/− PDGF-AA analyzed for *in vitro* wound closure (representative scratch assay shown) (n=3).
(I) Schematic representation of mechanism underlying GSDMB-mediated phosphorylation of FAK by PDGF-AA.
Significance for gene set enrichment analysis was determined using Cuffdiff, with a cutoff of P<0.05 after Benjamini Hochberg correction for multiple testing. Data presented as mean ± SEM, ns P≥ 0.01; *P<0.05, **P<0.01, ***P<0.001, ****P<0.0001 vs. Cont., $^{\#}P$<0.05, $^{\#\#\#}P$<0.001, $^{\#\#\#\#}P$<0.0001 vs. *GSDMB*$^{-/-}$ (unless otherwise noted) by one-way ANOVA with multiple comparisons. All experiments were repeated three times and yielded consistent results.

Key resources table

REAGENT or RESOURCE	SOURCE	IDENTIFIER
Antibodies		
anti Gasdermin B	Sigma Aldrich	HPA052407
anti Gasdermin B	Sigma Aldrich	HPA023925
anti CD326 (EpCAM)	Invitrogen	14-9326-82
anti Caspase 1	Abcam	EPR16883
anti Caspase 3	Abcam	AB32351
anti Caspase 7	Cell Signaling	12827
anti Caspase 8	Invitrogen	MA5-15226
anti Gasdermin D	Sigma Prestige Antibodies	HPA033387
anti E-Cadherin	BD Transduction Laboratories	610181
anti AIF	Cell Signaling	5318
anti Histone H3	Cell Signaling	4499
anti NM IIA	Biolegend	908901
anti Vinculin	BD Bioscience	550513
anti Phospho. FAK (Tyr397)	Cell Signaling	8556
anti FAK	Cell Signaling	3285
anti SRC	Cell Signaling	2123
anti Phospho.SRC (Tyr118)	Cell Signaling	2101
anti Paxillin	Cell Signaling	12065
anti Alpha actinin	Cell Signaling	6487
anti Tensin 2	Cell Signaling	4021
anti Hsp60	Cell Signaling	4870
anti GAPDH	Cell Signaling	14C10
anti Rabbit secondary	Cell Signaling	7074S
Alexa Fluor™ 594 Donkey anti-Rabbit	Invitrogen	A21207
Alexa Fluor™ 488 Donkey anti-mouse	Abcam	AB150105
Alexa Fluor™ 594 Donkey anti-Rabbit	Invitrogen	A21206
Alexa Fluor™ 488 Donkey anti-mouse	Invitrogen	A31570
Bacterial and virus strains		
Biological samples		
Human intestinal IBD biopsies (UC and CD)	Laikon Hospital (Athens)	Table S2
Human intestinal control biopsies	Laikon Hospital (Athens)	Table S2
Human IBD IECs (UC and CD)	Cleveland DDRCC	Table S2
Human control IECs	Cleveland DDRCC	Table S2
Human IBD colonoids	Cleveland Clinic Foundation	Table S2
Human control colonoids	Cleveland Clinic Foundation	Table S2
Chemicals, peptides, and recombinant proteins		

REAGENT or RESOURCE	SOURCE	IDENTIFIER
HEPES	Santa Cruz	Sc-29097A
Triton X-100	Thermo Fisher Scientific	BP151
Methanol	Thermo Fisher Scientific	A452SK-4
Xylene	Thermo Fisher Scientific	XS-1
Tween-20	Thermo Fisher Scientific	BP151
Tris Base	Thermo Fisher Scientific	BP152
Glycine	Thermo Fisher Scientific	BP381
Dithiothereitol (DTT)	Thermo Fisher Scientific	BP172
Sodium Bicarbonate	Millipore Sigma	S5761
SIGMA FAST protease inhibitor Cocktail Tablets EDTA free	Millipore Sigma	S8830
Hydrogen Peroxide	Thermo Fisher Scientific	H325-500
RNA*later*™ Solution	Invitrogen	AM7021
Paraformaldehyde	Millipore Sigma	158127
10% Formalin	Millipore Sigma	HT501128-4L
Fetal Bovine Serum, Certified	Gibco	16000036
SuperCalf Serum	Gemini Bio-Products	100-510
Penicillin/streptomycin	Gibco	15140122
Antibiotic/antimyotic (100X)	Invitrogen	15240062
Hank’s Balanced Salt Solution (HBSS)	Gibco	14175095
PBS	Gibco	10010023
MEM Amino Acid (50X)	Gibco	11130051
McCoy’s 5A medium + L-glutamine and sodium bicarbonate	Millipore Sigma	M4892-10
DMEM	Corning	10-017
Advanced DMEM	Thermo Fisher Scientific	12491015
Glutamax 100X	Gibco	35050061
0.25% Trypsin-EDTA	Thermo Fisher Scientific	25200056
0.05% Trypsin-EDTA	Thermo Fisher Scientific	25300054
TrypLE Express Solution	Gibco	12605
Matrigel®	Corning	356255
Wnt3a	Millipore Sigma	H17001-10UG
R-spondin 3	R&D Systems	3500-RS
Noggin	Stem Cell	78060.2
L-WRN Conditioned Media Supplement	Millipore Sigma	SCM105
B27	Thermo Fisher Scientific	17504044
N-2	Thermo Fisher Scientific	17502048
N-acetylcysteine	Millipore Sigma	A9165
EGF	Stem Cell	78006.2
Gastrin	Tocris	3006
A 83-01	R&D Sytems	2939

REAGENT or RESOURCE	SOURCE	IDENTIFIER
Methotrexate (Mtx)	DOT Scientific	DSM63820-1
hrIFNγ	R&D Systems	285-IF-100/CF
hrTGFβ	R&D Systems	240-B-500/CF
hrTNFα	R&D Systems	210-TA-100/CF
hrIL-33	R&D Systems	3625-IL-10/CF
Flagellin	Novus Bio	NBP2-35885
Dextran Sodium Sulfate (DSS)	TdB Consultancy AB	9011-18-1
ZINC40099027	AOBIOUS	CAS 1211825-25-0
hrPDGF-AA	Origene	NM_002607
LPS	Millipore SIgma	L2630-25MG
Nigericin	Millipore Sigma	SML1779-1ML
Formalin Phosphate	Thermo Fisher Scientific	SF100-4
Saponin	Millipore Sigma	S4521
Bovine Serum Albumin (BSA)	Millipore Sigma	A7030-50G
Normal goat serum	Abcam	Ab7481
Avidin-biotin complex (ABC)	Vector Laboratories	PK-6100
Diaminobenzidine substrate	Vector Laboratories	SK-4100
Harris Hematoxylin 1	Thermo Fisher Scientific	7721
Bluing Reagent	Millipore Sigma	XX0773
RT-PCR grade water	Invitrogen	9935g
FastStart Universal Probe Master (ROX)	Roche	04913957001
RIPA	Thermo Fisher Scientific	89900
PhosphoSafe™ Extraction Reagent	Millipore Sigma	71296-4
TaqMan Genotyping Master Mix	Applied Biosystem	4371355
NEB Buffer 2.0	New England Biolabs	NEB B7202
Px459 (Puro)	Addgene	62988
DH5-α	Thermo Fisher Scientific	C449601
Lipofectamine™ 3000	Invitrogen	L3000001
G418	Invitrogen	10131053
pGEM-T	Promega	A3600
Puromycin	Millipore Sigma	P9620
pMD2.G	Addgene	12259
psPAX	Addgene	12260
Polybrene Transfection Reagent	EMD Millipore Sigma	TR-1003-G
Propidium Iodide (PI)	Invitrogen	P1304MP
SYTOX Deep Red	Invitrogen	S11380
Click-iT™ EdU Cell Proliferation Kit	Invitrogen	C10337
Trypan Blue 0.4%	Gibco	15250061
Collagen I	Corning	354236

REAGENT or RESOURCE	SOURCE	IDENTIFIER
ProLong™ Gold Antifade Mountant with DAPI	Invitrogen	P36934
Critical commercial assays		
LookOut Mycoplasma PCR Detection Kit	Millipore SIgma	MP0040A
High Pure RNA Isolation Kit	Roche Life Science	11828665001
AllPrep® DNA/RNA/Protein Mini Kit	QIAGEN	80004
High-Capacity RNA-to-cDNA™ Kit	Applied Biosystems	4387406
Cell Fractionation Kit	Cell Signaling	9038S
Pierce™ BCA Protein Assay Kit	Thermo Fisher Scientific	23225
cyQUANT™ LDH Cytotoxicity Assay	Invitrogen	C20300
Click-iT™ EdU Cell Proliferation Kit	Invitrogen	C10337
Crystal Violet Cytotoxicity Kit	BioVision	K329-1000
PDGF-AA ELISA	RayBiotech	ELH-PDGFAA-1
PDGF-AB ELISA	RayBiotech	ELH-PDGFAB-1
Deposited data		
scRNAseq	Corridoni et al., 2020	GSE148837
scRNAseq	Corridoni et al., 2020	GSE148505
RNAseq	This study	GSE191015
Experimental models: Cell lines		
HT-29	ATCC	HTB-38
HEK293T	ATCC	CRL-3216
Experimental models: Organisms/strains		
Oligonucleotides		
GSDMB	TaqMan™ Thermo Fisher Scientific	Hs00218565_m1
GAPDH	TaqMan™ Thermo Fisher Scientific	Hs02786624_g1
CASP1	TaqMan™ Thermo Fisher Scientific	Hs00354836_m1
IL1β	TaqMan™ Thermo Fisher Scientific	Hs01555410_m1
GSDMB SNP 299	TaqMan™ Thermo Fisher Scientific	4351379 rs2305479
GSDMB SNP 306	TaqMan™ Thermo Fisher Scientific	4351379 rs2305480
GSDMB GCCTTGTTATGCTGATAGAT	VectorBuilder	N/A
Recombinant DNA		
GSDMB	Horizon Discovery	MHS6278-202801340
Software and algorithms		
R package GEOquery	Davis and Meltzer, 2007	N/A

REAGENT or RESOURCE	SOURCE	IDENTIFIER
limma R package	Ritchie et al., 2015	N/A
Seurat package	Butler et al., 2018	N/A
DESeq2R package	Love et al., 2014	N/A
TrimGalore! V.0.4.2	Babraham Bioinformatics	N/A
STAR aligner v2.5.3	Dobin et al., 2013	N/A
Cufflinks v2.2.1	Trapnell et al., 2010	N/A
R package clusterProfiler	Yu et al., 2012	N/A
ggplot2 R package	https://ggplot2.tidyverse.org	N/A
QuantStudio 3 Real-Time PCR Systems	Applied Biosystem	N/A
ImageQuant™ LAS 4000	GE	N/A
TaqMan® Genotyper Software	https://www.thermofisher.com/pr/en/home/technical-resources/software-downloads/taqman-genotyper-software.html	N/A
GraphPad Prism	https://www.graphpad.com/scientific-software/prism/	N/A
ImageJ	Schneider et al., 2012	https://imagej.net/Welcome
Adobe Illustrator Creative Cloud	Adobe	https://www.adobe.com/creativecloud/plans.html?filter=design&plan=individual&promoid=YB1TGRTR&mv=other
Adobe Photoshop Creative Cloud	Adobe	https://www.adobe.com/creativecloud/plans.html?filter=design&plan=individual&promoid=YB1TGRTR&mv=other
Other		